Articles in PresS. Am J Physiol Lung Cell Mol Physiol (May 31, 2013). doi:10.1152/ajplung.00355.2012

Ezrin/radixin/moesin proteins differentially regulate endothelial hyperpermeability after thrombin

Djanybek M. Adyshev[1], Steven M. Dudek[1], Nurgul Moldobaeva[1], Kyung-mi Kim[2], Shwu-Fan Ma[3], Anita Kasa[2, 4], Joe G. N. Garcia[1], Alexander D. Verin[2]

[1]Institute for Personalized Respiratory Medicine, Department of Medicine, Section of Pulmonary, Critical Care, Sleep, and Allergy, University of Illinois at Chicago, Chicago, Illinois, USA 60612
[2] Vascular Biology Center, Georgia Health Sciences University, Georgia, USA 30912
[3]Section of Pulmonary and Critical Care Medicine, University of Chicago, Chicago, Illinois, USA 60637
[4]Department of Medical Chemistry, University of Debrecen Medical and Health Science Center, Debrecen, H-4032, Egyetem tér 1, Hungary

Running head: ERM proteins and hyperpermeability

Corresponding author:

Djanybek M. Adyshev, PhD
Institute for Personalized Respiratory Medicine
Section of Pulmonary, Critical Care, Sleep, and Allergy
University of Illinois at Chicago
COMRB 3154, MC 719
909 S. Wolcott Avenue
Chicago, IL 60612
Phone : 312-355-5933
Fax : 312-996-7193
Email : dadyshev@uic.edu

Abstract

Endothelial cell (EC) barrier disruption induced by inflammatory agonists such as thrombin leads to potentially lethal physiological dysfunction such as alveolar flooding, hypoxemia and pulmonary edema. Thrombin stimulates paracellular gap and F-actin stress fiber formation, triggers actomyosin contraction and alters EC permeability through multiple mechanisms that include protein kinase C (PKC) activation. We previously have shown that the ezrin, radixin, and moesin (ERM) actin-binding proteins differentially participate in S1P-induced EC barrier enhancement. Phosphorylation of a conserved threonine residue in the C terminus of ERM proteins causes conformational changes in ERM to unmask binding sites and is considered a hallmark of ERM activation. In the present study we test the hypothesis that ERM proteins are phosphorylated on this critical threonine residue by thrombin-induced signaling events and explore the role of the ERM family in modulating thrombin-induced cytoskeletal rearrangement and EC barrier function. Thrombin promotes ERM phosphorylation at this threonine residue (Ezrin-567, Radixin-564, Moesin-558) in a PKC-dependent fashion and induces translocation of phosphorylated ERM to the EC periphery. Thrombin-induced ERM threonine phosphorylation is likely synergistically mediated by protease-activated receptors PAR_1 and PAR_2. Using the siRNA approach, depletion of either moesin alone, or of all three ERM proteins, significantly attenuates thrombin-induced increase in EC barrier permeability (TER), cytoskeletal rearrangements, paracellular gap formation and accumulation of di-phospho-MLC. In contrast, radixin depletion exerts opposing effects on these indices. These data suggest that ERM proteins play important differential roles in the thrombin–induced modulation of EC permeability, with moesin promoting barrier dysfunction and radixin opposing it.

Keywords: thrombin; ERM; PKC; phosphorylation; endothelial cells; barrier dysfunction; cytoskeleton

90 **Abbreviations:** ERM, ezrin, radixin, and moesin proteins; PKC, protein kinase C; Thr, thrombin

91

Introduction

The pulmonary vascular endothelium serves as a semi-selective barrier between circulating blood and surrounding tissues. Endothelial cell (EC) barrier integrity is therefore critical to tissue and organ function. Disruption of the endothelial barrier by inflammatory mediators such as thrombin, histamine, and LPS leads to potentially lethal physiological dysfunction such as hypoxemia, atherosclerosis and pulmonary edema, a hallmark of acute lung injury and its more severe form, acute respiratory distress syndrome (12). Therefore, the preservation of vascular endothelial cell (EC) barrier integrity has the potential for profound clinical impact. Multiple studies have demonstrated that inflammation-induced EC barrier dysfunction involves cytoskeletal rearrangement, contraction of endothelial cells and intercellular gap formation, leading to increased paracellular permeability (18, 20, 55, 65). Thrombin, a multifunctional serine protease, proteolytically cleaves and activates PAR_1, a member of a unique class of G protein–coupled receptors activated by proteolytic cleavage of their extracellular N-terminal domains and expressed at the surfaces of EC (43, 66). Thrombin can transactivate PAR_2 through PAR_1 in cultured human umbilical vein EC (HUVECs) (48). PAR_1 and PAR_2 activate heterotrimeric G-proteins G_q, $G_{12/13}$, and G_i, all of which are involved in permeability regulation (42). Activation of G_q mobilizes Ca^{2+} and activates PKC, RhoA, and EC contraction, resulting in endothelial barrier disruption.

The widely distributed ERM family of membrane-associated proteins (ezrin, radixin, moesin) regulates the structure and function of specific domains of the cell cortex [reviewed in (2, 14, 46)]. The ERM proteins are actin-binding linkers that connect the actin cytoskeleton to the plasma membrane. This linker function makes ERM proteins essential for many fundamental cellular processes including cell adhesion, determination of cell shape, motility, cytokinesis and integration of membrane transport with signaling pathways (14, 47, 71). The three ERM proteins

share a high level of amino acid identity (70-85%) (14), and prior to activation exist in an auto-inhibited conformation in which the actin-binding C-terminal tail binds and masks the N-terminal FERM domain (band 4.1, ezrin, radixin, moesin homology domains) (50). The activation state of ERM proteins is tightly regulated by phosphorylation events. Binding of the protein to membrane lipid phosphatidylinositol 4,5-bisphosphate (PIP_2) (15) and subsequent phosphorylation of a conserved C-terminal threonine (T567 in ezrin, T564 in radixin, T558 in moesin) (21, 41, 50) are believed to disrupt the intramolecular association, thus unmasking sites for interactions with other proteins. In addition, phosphorylation of ezrin on other residues may be required to direct specific targeted effects in cells (29, 36, 57). Several kinases have been implicated in regulating ERM protein function through phosphorylation of the C-terminal threonine residue (3, 10, 35, 40, 59, 67). However, the identity of kinases that directly phosphorylate ERM in many cells remains to be clearly defined (14, 29).

ERM proteins also associate with cytoplasmic signaling molecules in cellular processes that require membrane cytoskeletal reorganization. ERM proteins appear to act both downstream and upstream of the Rho family of GTPases, which regulates remodeling of the actin cytoskeleton (14, 29). However, information is limited concerning the possible role of ERM proteins in the remodeling of endothelial cytoskeleton in response to different agonists. Koss and coworkers (35) demonstrated that ERM proteins are phosphorylated on C-terminal threonine residues by TNF-α-induced signaling events and likely play important roles in modulating the cytoskeletal changes and permeability increases in human pulmonary microvascular EC. We previously have shown that PKC isoforms are required for ERM phosphorylation in human pulmonary EC induced by the potent barrier protective factor, platelet-derived phospholipid sphingosine-1 phosphate (S1P) (1). Further, we previously demonstrated that ERM proteins,

despite their structural similarities and reported functional redundancy, differentially modulate S1P-induced changes in lung EC cytoskeleton and permeability (1). In the present study, we explored the potential involvement of ERM proteins in modulating thrombin-induced cytoskeletal rearrangement and EC barrier function.

Materials and methods

Reagents

Thrombin was obtained from Sigma Co. (St. Louis, MO). Antibodies (Ab) were obtained as follows: mouse monoclonal Ab against β-Tubulin (Covance, Berkeley, CA), rabbit polyclonal di-phospho-MLC and rabbit polyclonal phospho-Ezrin (Thr567)/Radixin (Thr564)/Moesin (Thr558) Ab (Cell Signaling, Danvers, MA), ezrin specific mouse monoclonal Ab (Invitrogen Life Technologies, Carlsbad, CA), rabbit monoclonal anti-radixin Ab (Sigma, St. Louis, MO), mouse monoclonal anti-moesin Ab (BD Biosciences, San Jose, CA), mouse monoclonal anti-thrombin receptor WEDE15 blocking Ab (Beckman Coulter, Indianapolis, IN), mouse monoclonal thrombin R (ATAP2) blocking Ab (Santa Cruz Biotech., Santa Cruz, CA), Texas red phalloidin and Alexa 488-, Alexa 594-conjugated secondary Ab (Molecular Probes, Eugene, OR). ROCK inhibitors Y-27632 and H-1152, PKC inhibitors Ro-31-7549, Bisindolylmaleimide I, and Go 6976, p38 kinase inhibitor SB203580 were purchased from Calbiochem (San Diego, CA), $Ca^{(2+)}$ chelator BAPTA-AM was obtained from Sigma (St. Louis, MO), PI3 Kinase inhibitor LY294002 and MLCK inhibitor ML-7, PAR_1 selective agonist TFLLR-NH_2, PAR_2 selective agonist SLIGRL-NH_2 and reversed amino acid sequence control peptides RLLFT-NH_2

and LRGILS-NH_2 were obtained from TOCRIS (Bristol, UK). Unless specified, biochemical reagents were obtained from Sigma.

Cell culture

Human pulmonary artery endothelial cells (HPAEC) were obtained from Lonza Inc. (Walkersville, MD) and were utilized at passages 5–9.

Measurement of transendothelial electrical resistance

Cellular barrier properties were measured using an electrical cell substrate impedance sensing system (ECIS) (Applied Biophysics, Troy, NY). HPAEC were seeded onto plates with small gold electrodes (10–4 cm^2) and measurements of transendothelial electrical resistance (TER) across confluent HPAEC monolayers were performed as previously described (6, 19, 65).

Real-time quantitative RT–PCR

Endogenous transcript levels of ezrin (*EZR*), radixin (*RDX*), and moesin (*MSN*) in HPAEC were measured in a 384-well PCR plate with an ABI 7900 HT Fast Real-Time PCR System (Applied Biosystems, Carlsbad, CA). Total RNA (1 μg) were first reverse transcribed using Superscript II Reverse Transcriptase (Invitrogen Life Technologies) and random hexamer primers (Applied Biosystems) to generate cDNA. Quantitative Real Time-PCR (qRT-PCR) was then performed using the Assay-on-Demand system (Hs00185574_m1 (*EZR*); Hs00267954_m1 (*RDX*); Hs00792607_mH (*MSN*) from Applied Biosystems according to the manufacturer's protocol. Purity and specificity of all products were confirmed by omitting the reverse transcriptase or template. Analysis of results is based on the average of triplicates. The standard

curve method was used for relative quantitation of target gene expression. Further information on the method can be found on User Bulletin #2 on the ABI website.

Depletion of specific EC proteins via siRNA

To reduce the content of individual EC proteins, cultured EC were treated with specific siRNA duplexes, which guide sequence-specific degradation of the homologous mRNA (13). The following validated siRNAs were obtained from QIAGEN (Valencia, CA) in ready-to-use, desalted, and duplexed form: duplex of sense 5′-CACCGUGGGAUGCUCAAAGdTdT-3′ and antisense 5′-CUUUGAGCAUCCCACGGUGdTdT-3′ siRNA was used for targeting sequences that are part of the coding region for Homo sapiens ezrin: 5′-AACACCGTGGGATGCTCAAAG-3′, duplex of sense 5′-GAAAUAACCCAGAGACUCUdTdT-3′ and antisense 5′-AGAGUCUCUGGGUUAUUUCdTdT-3′ was used for targeting sequences that are part of the coding region for Homo sapiens radixin: 5′-AAGAAATAACCCAGAGACTCT-3′, and duplex of sense 5′-GGGAUGUCAACUGACCUAAdTdT-3′ and antisense 5′-UUAGGUCAGUUGACAUCCCdTdG-3′ was used for targeting sequences that are part of the coding region for Homo sapiens moesin: 5′-CAGGGATGTCAACTGACCTAA-3′. Duplex of sense 5′-AGAGCUAAG-UAGAUGUGUAdTdT-3′ and antisense 5′-UACACAUCUACUUAGCUCUdTdG-3′ siRNA was used for targeting sequences that are part of the coding region for Homo sapiens PKCβI: 5′-CAAGAGCTAAGTAGATGTGTA-3′, duplex of sense 5′-GAAGCAUGACAGCAUUAAA dTdT-3′ and antisense 5′-UUUAAUGCUGUCAUGCUUCdCdG-3′ was used for targeting sequences that are part of the coding region for Homo sapiens PKCζ: 5′-CGGAAGCATGACAGCATTAAA-3′, duplex of

sense 5′-CUCUACCGUGCCACGUUUUdTdT-3′ and antisense 5′-AAAACGUGGCACGGUAGAGdTdT-3′ was used for targeting sequences that are part of the coding region for Homo sapiens PKCδ: 5′-AACTCTACCGTGCCACGTTTT-3′, duplex of sense 5′-CAAGAAGUGUAUUGAUAAAdTdT-3′ and antisense 5′-UUUAUCAAUACACUUCUUGdTdG-3′ was used for targeting sequences that are part of the coding region for Homo sapiens PKCθ: 5′-CACAAGAAGTGTATTGATAAA-3′, duplex of sense 5'- CGGAAACACCCGUACCUUAdTdT-3' and antisense 5'-UAAGGUACGGGUGUUUCCGdTdG-3' were used for targeting sequences that are part of the coding region for Homo sapiens PKCε: 5'- CACGGAAACACCCGTACCTTA-3'. Silencer select pre-designed siRNA duplex (Life Technologies, Grand Island, NY) of sense 5'-CCCGUAACCUAAUUCCUAUdTdT-3' and antisense 5'-AUAGGAAUUAGGUUACGGGdCdC-3' was used for targeting sequences that are part of the coding region for Homo sapiens PKCγ: 5'- GGCCCGTAACCTAATTCCTAT-3'. Non-specific, non-targeting AllStars siRNA duplex (QIAGEN, Valencia, CA) was used as negative control treatment. HPAEC were grown to 70% confluence, and the transfection of siRNA (final concentration 50 nM) was performed using DharmaFECT1 transfection reagent (Dharmacon Research, Lafayette, CO) according to manufacturer's protocol. Forty eight hours post-transfection cells were harvested and used for experiments. Additional control experiments using EC transfections with fluorescently labeled nonspecific RNA showed that this protocol allowed us to achieve 90–100% transfection efficiency.

Plasmid Constructs

Moesin constructs (wild type and phosphorylation deficient mutant) were prepared as we have previously described (9).

Immunofluorescent staining

EC were plated on glass coverslips, grown to 70% confluence, and transfected with siRNA followed by stimulation with thrombin. Then cells were fixed in 3.7% formaldehyde solution in PBS for 10 min at 4°C, washed three times with PBS, permeabilized with 0.2% Triton X-100 in PBS-Tween (PBST) for 30 min at room temperature, and blocked with 2% BSA in PBST for 30 min. Incubation with antibody of interest was performed in blocking solution for 1 h at room temperature followed by staining with either Alexa 488-, or Alexa 594-conjugated secondary Ab (Molecular Probes). Actin filaments were stained with Texas Red-conjugated phalloidin (Molecular Probes) for 1 h at room temperature. After immunostaining, the glass slides were analyzed using a Nikon video-imaging system (Nikon Instech Co., Japan) consisting of a phase contrast inverted microscope Nikon Eclipse TE2000 connected to Hamamatsu (Hamamatsu Photonics K.K., Japan) digital camera and image processor. The images were recorded and processed using Adobe Photoshop 6.0.

Immunoblotting

Protein extracts were separated by 4-15% gradient SDS-PAGE, transferred to nitrocellulose or polyvinylidene difluoride membranes (30 V for 18 h or 100 V for 1.5 h), and reacted with Ab that recognizes ezrin, moesin, radixin, or other Ab of interest as indicated for individual experiments. The level of phosphorylated ERM was examined by using a single Ab that recognizes any of the three ERM proteins only when they are phosphorylated on the threonine

253 residue: ezrin (T567)/radixin (T564)/moesin (T558) (Cell Signaling). Immunoreactive proteins
254 were detected with the enhanced chemiluminescent detection system (ECL) according to the
255 manufacturer's directions (Amersham, Little Chalfont, UK). Intensities of immunoreactive
256 protein bands were quantified using ImageQuant software (Molecular Dynamics, Sunnyvale,
257 CA).
258
259 **Statistical Analysis**
260 Results are expressed as means ±SD of three to six independent experiments. We
261 performed statistical comparison among treatment groups by unpaired Student's t-test or by
262 randomized-design two-way analysis of variance followed by the Newman-Keuls post hoc test
263 for multiple-groups. Results with $P < 0.05$ were considered statistically significant.
264
265 **Results**
266 **Expression of ezrin, radixin and moesin in HPAEC**
267 The mRNA expression profiles of individual ERMs were analyzed for confluent human
268 pulmonary EC. RT-PCR analysis reveals differential expression with highest relative expression
269 of moesin and lowest expression of radixin (Fig.1).
270
271 **Thrombin induces threonine phosphorylation of ERM via a PKC-mediated pathway**
272 To elucidate the effect of thrombin on phosphorylation of ERM at its critical C-terminal
273 threonine, confluent human pulmonary EC were stimulated with thrombin (0.5 U/ml), and
274 threonine phosphorylation then was evaluated by Western blot analysis utilizing phospho-
275 specific ERM antibody (phospho-Ezrin Thr567/Radixin Thr564/Moesin Thr558). Thrombin

induced the sustained threonine phosphorylation of ERM, which reached maximum levels by 5 min and remained elevated for at least 120 min (Fig. 2).

Because several kinases, including members of PKC, ROCK, GRK2, p38, Mst4 and LOK, have been reported to phosphorylate the regulatory C-terminal threonine residue of ERM proteins in various systems (3, 10, 35, 40, 59, 67), experiments were performed to determine the signaling mechanisms leading to ERM phosphorylation in pulmonary EC upon thrombin treatment. The role of different kinases was examined by using specific pharmacological inhibitors: PKC-specific inhibitor Ro-31-7549, p38 MAPK inhibitor SB203580, Rho-associated protein kinase (ROCK) inhibitor Y-27632, phosphoinositide 3-kinases (PI3Ks) inhibitor LY294002, and chelator of intracellular Ca^{2+} BAPTA (Fig. 3). In our experiments, pretreatment with Ro-31-7549 effectively prevented the increase in ERM phosphorylation induced by thrombin (Fig. 3A), suggesting that this increase is PKC-dependent. Pretreatment with BAPTA, a chelator of intracellular Ca^{2+}, partially inhibited ERM phosphorylation (Fig. 3A). We next explored whether additional signaling pathways previously reported to participate in ERM regulation are involved in thrombin-induced ERM phosphorylation. Pretreatment with Y-27632 did not exert a significant effect on ERM threonine phosphorylation. At the same time, phosphorylation of myosin light chain (MLC), regulated by the ROCK/myosin phosphatase-dependent signaling pathway, was significantly attenuated in ECs preincubated with Y-27632 (Fig. 3A). Because of the critical role of Rho activation, through its downstream effector ROCK, in thrombin-induced EC barrier dysfunction, we next studied how the inhibition of ROCK affects ERM phosphorylation using the more potent and selective cell-permeable pharmacological ROCK inhibitor H-1152. Pretreatment with either H-1152 or Y-27632 did not exert significant effects on ERM threonine phosphorylation after thrombin (Fig. 3B). In addition, preincubation of

299 HPAEC with the pharmacologic inhibitor of p38 MAPK SB203580 did not significantly affect
300 ERM phosphorylation (Fig. 3A, B).

301 The role of PKC isoforms was examined by using two alternative approaches: pretreatment
302 of EC with PKC-specific pharmacological inhibitors and using isoform-specific siRNAs. We
303 utilized three PKC-specific pharmacological inhibitors that have different IC_{50} values for
304 different PKC isoforms, bisindolylmaleimide I (BIM), Go 6976, and Ro-31-7549. Bis I, Ro-31-
305 7549 and Go 6970 are all competitive inhibitors for the ATP-binding site of PKC (39, 63, 69).
306 BIM inhibits the conventional PKC isoforms α, βI, βII and γ (activated by phosphatidylserine,
307 diacylglycerol and Ca^{2+}) with similar potency (IC_{50} = 10 nM) (63), and the unconventional
308 isoforms δ and ε (require phosphatidylserine and diacylglycerol but are Ca^{2+}-independent) and
309 the atypical isoform ζ (require only phosphatidylserine), to a lesser extent (39). In contrast to
310 BIM, Ro-31-7549 has slight selectivity for the α isoform (IC_{50} = 53 nM), but also affects βI, βII,
311 ε and γ (69). Go 6970 inhibits Ca^{2+}-dependent PKC isoforms α and βI (39). In our experiments,
312 pretreatment with Ro-31-7549, BIM and Go 6970 effectively suppressed ERM phosphorylation
313 induced by thrombin (Fig. 3C). These pharmacological PKC inhibitor data combined with the
314 BAPTA data suggest that multiple PKC isoforms may be required. Furthermore, our experiments
315 demonstrate that incubation with Go 6976 significantly inhibited phosphorylation of MLC at
316 Thr18 and Ser19 induced by thrombin (Fig. 3C).

317 To better characterize the PKC isoforms involved in ERM phosphorylation after
318 thrombin, activation of individual PKC kinases was explored using isoform-specific phospho-
319 antibodies. Thrombin stimulation (0.5 U/ml) of HPAEC significantly increased phosphorylation
320 of PKCβ (Thr500) (Fig. 4A), PKCγ (Thr514) (Fig. 4B), PKCε (Ser729) (Fig. 4C),
321 PKCζ (Thr410) (Fig. 4D), PKCθ (Thr538) (Fig. 4E), and PKCδ (Tyr311) (Fig. 4F). Previous

studies have indicated that these PKC isoforms play important roles in thrombin- and other inflammatory agonists- (TNF-α, IL-1β, VEGF**,** hypoxia) induced modulation of endothelial permeability (16, 38, 44, 51, 53, 56, 61, 62, 70) and therefore were selected for further experimentation using isoform-specific siRNA. We first validated that these siRNAs efficiently inhibit their respective targets: 65±7% depletion of PKCβ, 97±2.2% depletion of PKCδ, 75.5±2.4% depletion of PKCθ, 92±2.5% depletion of PKCε, and 65±2.5% depletion of PKCγ [Fig. 5, see also (1)]. It is important to note the limitations of this siRNA approach as it does not provide 100% protein suppression and therefore some, albeit reduced protein function likely remains. EC were transfected with siRNA for PKCβI, PKCγ, PKCε, PKCζ, PKCθ or PKCδ and then stimulated with thrombin to determine the effects on ERM threonine phosphorylation. Depletion of individual PKCγ, PKCε, PKCζ, PKCθ or PKCδ isoforms significantly reduced ERM phosphorylation after thrombin (Fig. 6 A, B). To further clarify the involvement of PKC activity in thrombin-induced ERM and MLC phosphorylation, we pursued simultaneous depletion of several PKC isoforms (pan-PKC) via siRNA. Combined depletion of several PKC isoforms markedly reduced ERM phosphorylation after thrombin (Fig. 6C, D), suggesting possible cooperative regulation in this phosphorylation response. Moreover, downregulation of pan-PKC significantly attenuates thrombin-induced MLC di-phosphorylation (Fig. 6C, E), suggesting that multiple PKC isoforms may be involved. Taken together, these data indicate that multiple PKC isoforms (conventional, unconventional and atypical) likely participate in thrombin-induced ERM and MLC phosphorylation. One limitation of these data is that combined silencing of multiple PKC isoforms may result in some nonspecific effects, e.g. nonspecific activation or/and inhibition of other signaling pathways. Therefore, further studies utilizing

alternative approaches (e.g. isoform specific PKC peptide inhibitors) will be needed to verify these findings.

Effects of ERM depletion on thrombin-induced ERM threonine and MLC phosphorylation

Numerous studies have reported a critical role for activation of the contractile apparatus in specific models of agonist-induced EC barrier dysfunction [reviewed in (12)]. A key contractile event in thrombin-induced barrier dysfunction is the phosphorylation of regulatory MLC, catalyzed by Ca^2/CaM-dependent MLCK (60, 72) and regulated by small GTPase Rho. There are no antibodies currently available that specifically differentiate among the C-terminal phospho-threonines of individual ERM proteins. Therefore, to assess the contribution of individual proteins in total ERM threonine phosphorylation and their roles in MLC phosphorylation after thrombin, we used siRNAs targeting ezrin, radixin, and moesin. We first validated that these siRNAs efficiently and specifically inhibited their respective targets (1). Pulmonary EC were then transfected with nonspecific siRNA, or siRNA for moesin, radixin, or siRNA for the combination of ezrin, radixin and moesin (pan-ERM), and then stimulated with thrombin. Pan-ERM and MLC phosphorylation was evaluated by Western blot analysis utilizing phospho-specific ERM antibody and phospho-myosin light chain 2 (Thr18/Ser19) antibody (di-phospho-MLC). In contrast to cells transfected with nonspecific RNA, depletion of moesin alone or downregulation of pan-ERM significantly reduced time-dependent ERM and MLC phosphorylation after thrombin (Fig. 7A, D). Thrombin-induced ERM and MLC phosphorylation was partially attenuated by depletion of ezrin (Fig. 7C). In contrast, depletion of radixin did not have any significant effect on MLC phosphorylation after thrombin (Fig. 7B). Radixin siRNA partially, but significantly, reduced ERM threonine phosphorylation (Fig. 7B). Taken together,

these data indicate that in pulmonary EC thrombin induces primarily threonine phosphorylation of moesin, followed by ezrin, and then radixin. These data also suggest that activated moesin and to a lesser degree ezrin, but not radixin, may play a role in MLC phosphorylation induced by thrombin via the ROCK/myosin phosphatase signaling pathway.

Role of ERM in thrombin-induced lung EC hyperpermeability

To evaluate the functional involvement of individual ERM proteins in thrombin-induced EC barrier dysfunction, we measured changes in TER, a highly sensitive *in vitro* assay of permeability, in lung EC treated with nonspecific siRNA or those treated with siRNA for ezrin, radixin, or moesin (either singly or in combination). Comparing the data expressed as normalized resistance (Fig. 8) to the time course of ERM threonine phosphorylation (Fig. 2) demonstrates that the increase in ERM phosphorylation is highly correlated with the onset of thrombin-induced hyperpermeability. Depletion of individual ERM proteins does not affect basal permeability. However, the thrombin-induced decrease in TER is markedly attenuated in EC transfected with moesin or pan-ERM-specific siRNA (Fig. 8A, D and E) compared with cells transfected with nonspecific RNA duplexes. The initial thrombin-induced decrease in TER was attenuated by siRNA depletion of ezrin, but this intervention markedly enhanced the recovery above baseline in the later stage (Fig. 8C, E). In contrast, depletion of radixin slightly augments the decrease in TER during the early phase and attenuates the later recovery phase after thrombin (Fig. 8B, E) compared with agonist-stimulated cells transfected with nonspecific RNA. These data clearly indicate differential roles for individual ERM proteins in mediating thrombin-induced lung EC hyperpermeability.

Role of PARs in thrombin-induced ERM phosphorylation

In human pulmonary EC, activation of PAR_1 and PAR_2 promotes PKC and RhoA activation and triggers the endothelial barrier-disruptive response (7, 22, 37, 43). We next utilized PAR_1-specific blocking antibodies ATAP2 and WEDE15, and PAR_1 (TFLLR-NH_2) and PAR_2 (SLIGRL-NH_2) selective agonist peptides, to determine the roles of these receptors in thrombin-induced threonine phosphorylation of ERM. HPAEC preincubation with both ATAP2 and WEDE15, either singly or in combination, significantly decreased ERM phosphorylation after thrombin relative to controls (Fig. 9). Stimulation of EC with both TFLLR-NH_2 and SLIGRL-NH_2 augmented the phospho-ERM signal (Fig. 10) compared with cells treated with control peptides. Interestingly, incubation of EC with a combination of TFLLR-NH_2 and SLIGRL-NH_2 markedly enhanced ERM phosphorylation, compared with cells treated with these two agonists alone (Fig. 10), suggesting that both PAR_1 and PAR_2 may have additive or synergistic effects in this phosphorylation response.

Involvement of ERM in thrombin-induced EC cytoskeletal remodeling

Compromised barrier function induced by thrombin is tightly associated with actin cytoskeletal rearrangements, F-actin stress fiber formation, increased MLCK-catalyzed MLC phosphorylation spatially co-localized with stress fibers, actomyosin contraction, opening of paracellular gaps, and hyperpermeability (12, 43). Within this context, the distribution of phosphorylated ERM in EC before and after thrombin treatment was examined via immunofluorescence. Before thrombin treatment, minimal phosphorylated ERM was observed in the cytoplasm of pulmonary EC. In some areas of quiescent monolayers, phospho-ERM localized in the spike-like structures overlapping the cell-cell contact areas (Fig. 11, image a,

arrow 1). Stimulation with thrombin induced an increase in the amount of phosphorylated ERM, consistent with immunoblotting studies (Fig. 2). During the early response (5 minutes after initial stimulation), phosphorylated ERM was localized primarily at the cell periphery and spike-like areas (Fig. 11, image b, arrows 1 and 2) with a smaller amount of phospho-ERM also observed in the cytoplasm (Fig. 11, image b). In contracting EC (15 minutes after initial challenge) the phospho-ERM signal markedly increased in the peripheral cytoplasmic areas (Fig. 11, image c). During partial restoration phases (60 and 120 minutes after the initial challenge), phosphorylated ERM primarily localized in cytoplasmic areas and spike-like structures that were originally seen in quiescent cells (Fig. 11, images d, e), but the overall level of phosphorylated ERM appeared slightly elevated compared to baseline. These dynamic changes in phosphorylated ERM localization during the phases of active cell contraction and partial barrier restoration indicate that ERM proteins may play a role in both processes. The observation that phosphorylated ERM proteins were primary concentrated along the EC periphery upon thrombin treatment led us to examine the role of these proteins in modulating endothelial cytoskeletal rearrangements that occur during thrombin-induced EC hyperpermeability.

In the next series of experiments we analyzed the effect of ERM depletion on the human endothelial actin cytoskeleton. EC were transfected with nonspecific RNA duplex oligonucleotides (Fig. 12) or ERM-specific siRNA (Fig. 12) followed by thrombin challenge (15 min, 0.5 U/ml). Double immunofluorescent staining using Texas red phalloidin to visualize F-actin and di-phospho-MLC antibody to detect phosphorylated MLC was performed. Unstimulated EC transfected with ezrin-, radixin-, or moesin-specific siRNAs, either individually or in combination, demonstrated no significant differences in the organization of actin cytoskeleton and levels of MLC phosphorylation compared with control EC exposed to

nonspecific RNA (Fig. 12, panel A, images a-n). However, thrombin stimulation of EC treated with nonspecific RNA induced robust F-actin stress fiber and gap formation and accumulation of di-phospho-MLC (Fig. 12, panel B, images c and d), which were nearly abolished by the combination of siRNAs for radixin/ezrin/radixin (pan-ERM depletion), or by siRNA for moesin alone. In contrast, radixin depletion alone slightly *enhanced* stress fiber formation and MLC phosphorylation (Fig.12, panel B, images k and l). We next explored the effects of overexpression of a phosphorylation-deficient mutant of moesin (Thr558Ala) on EC cytoskeletal organization. Scanning densitometry (Fig. 13A) demonstrated relatively equivalent expression of the wild type and mutant moesin in EC. Monolayers overexpressing mutant moesin exhibited decreased F-actin stress fibers after thrombin and prominent cortical actin compared to EC overexpressing wild type moesin (Fig.13, panel B, images c, g). These data together demonstrate that ERM proteins are downstream targets of thrombin-induced signaling mechanisms and play an essential and differential role in the regulation of the endothelial actomyosin cytoskeleton.

Discussion

Prior work has revealed that the procoagulant serine protease thrombin induces endothelial barrier compromise through G protein-coupled Ca^{2+} mobilization, MLCK, PKC and RhoA activation, which produces cytoskeletal rearrangement, dissociation of endothelial cell-cell junctions as well as cytoskeleton contraction resulting in paracellular hyperpermeability (12, 27, 33, 34, 43, 45, 66). Although ERM proteins act as signal transducers for agonists that induce cytoskeletal remodeling (14), the role of ERM in barrier regulation by thrombin is unknown. Moesin is the most expressed ERM protein in several types of endothelial cells (4, 24, 30, 35). Here we demonstrate that moesin is the most abundant ERM expressed in HPAEC as measured by mRNA content, with radixin being the least expressed. We previously have shown that the

460 angiogenic sphingolipid S1P induces ERM phosphorylation on a conserved threonine residue
461 critical for ERM activation via a pathway that requires PKC, Rac1, Rho A, and p38 MAPK (1).
462 We also have previously demonstrated that phosphorylation of ERM in response to the
463 microtubule disruptor 2-methoxyestradiol (2ME) occurs in a p38/PKC-dependent manner
464 (9). We therefore explored whether the ERM family of proteins plays a role in modulating the
465 thrombin-induced endothelial barrier response**.** Our data demonstrate that thrombin increases
466 ERM phosphorylation at a critical regulatory threonine site in HPAEC monolayers and strongly
467 suggest important roles for the ERM proteins in mediating endothelial barrier dysfunction by
468 thrombin. This phosphorylation requires thrombin-induced signaling pathways that include
469 activation of PKC isoforms, but it is not regulated in a RhoA/ROCK- or p38-dependent manner.
470 Our results differ from those in our (1, 9), and others previous studies (23, 35, 68), in which the
471 phosphorylation of ERM was PKC-, RhoA/ROCK- and-p38-dependent in response to S1P,
472 PKC- and RhoA/ROCK-dependent in response to 2ME and TNF-α, and RhoA/ROCK-
473 dependent in response to advanced glycation end products (AGE). Together, these observations
474 suggest that ERM may be phosphorylated at the critical C-terminal threonine site by different
475 upstream pathways that can vary from endothelium to endothelium and from stimuli to stimuli.
476 We and others previously have demonstrated that several PKC isoforms - conventional,
477 unconventional and atypical—are likely to phosphorylate the C-terminal threonine residue of
478 ERM proteins (1, 35, 52, 67). Our data now demonstrate that PKC isoforms ζ, γ, ε, θ and
479 δ, which previously have been demonstrated to play roles in inflammation-induced changes in
480 endothelial permeability (16, 44, 53, 56, 61, 62, 70), participate in thrombin-induced ERM
481 phosphorylation at the C-terminal threonine site in human pulmonary EC (Figure 6). Moreover,
482 our data indicate that these isoforms may synergistically regulate both ERM threonine and MLC

phosphorylation (Fig. 6C, D). One of the key events in the signaling cascade triggered by thrombin binding to PAR receptors is Ca^{2+}-dependent activation of PKC and Ca^{2+}/calmodulin-dependent MLCK, which phosphorylates myosin light chain (MLC) (12, 37). RhoA and its effector ROCK indirectly regulate MLCK activation and MLC phosphorylation and therefore also mediate endothelial hyperpermeability in response to thrombin (8, 49, 64). The RhoA/ROCK pathway is one of the downstream signals activated by PKC (8). Data demonstrating that ERM are phosphorylated by PKC in response to thrombin prompted us to examine the time-dependent phosphorylation status of individual ERM and whether ERM play a role in MLC phosphorylation after thrombin. The effects of ERM siRNA treatment, either singly or in combination, on the phosphorylated ERM and MLC phosphorylation before or after thrombin treatment were examined. We discovered that all three proteins were phosphorylated; however, knockdown of moesin alone or all three ERM proteins together significantly reduced thrombin-induced ERM and MLC phosphorylation (0-90 minutes). In contrast, depletion of radixin did not have any significant effect on MLC phosphorylation while slightly reducing ERM threonine phosphorylation after thrombin. Depletion of ezrin partially attenuated thrombin-induced ERM and MLC phosphorylation. Importantly, these data demonstrate differential roles for the ERM proteins in response to thrombin, despite their structural similarities and reported functional redundancy. These data also clearly suggest that moesin and to a lesser degree ezrin, but not radixin, are critically involved in MLC phosphorylation after thrombin.

The underlying mechanism through which moesin and ezrin regulate MLC phosphorylation remains to be determined. ERM proteins are known to activate the Rho signaling in cell adhesion regulation via association with Rho regulator Rho GDP-dissociation inhibitor (GDI) (58). Our data indicate that ERM may be upstream of MLC phosphorylation. Depletion of PKC isoforms

506 (Fig. 6A-D) indicated that PKC-dependent moesin and ezrin phosphorylation on regulatory C-
507 terminal threonine is involved in thrombin-induced RhoA activation and subsequent increased
508 MLC phosphorylation. In addition, phosphorylation of moesin or/and ezrin at sites other then C-
509 terminal threonine may contribute to this activation. For example, several additional sites have
510 been reported for ezrin (threonine 235, tyrosines 145 and 353) (36, 73), but the functional roles
511 of phosphorylation at these sites are still unclear. Interestingly, as we recently have been reported
512 (31), each ERM protein has a distinct binding ability toward the subunits (CSIβ and MYPT) of
513 MLC phosphatase (MLCP), a type 1 protein phosphatase (PPase 1) that regulate reversible
514 phosphorylation of the MLC in intercellular gap formation and barrier dysfunction of EC. Our
515 data demonstrated that the catalytical subunit CSIβ preferably bound to moesin, while the band
516 that corresponds to ezrin detected in CSIβ immunoprecipitates is faint. In contrast, radixin did
517 not bind to CSIβ, but strongly interacted with MLCP targeting subunit MYPT I. It is possible,
518 that in addition to RhoA activation after thrombin, moesin may inhibit MLCP function leading to
519 increased MLC phosphorylation. Our prior results indicated that MLCP play an important role in
520 barrier protection in EC (31). Radixin may regulate MLCP activation through binding to MYPT
521 I in S1P-induced barrier enhancement. Future studies will be needed to clarify the link between
522 PKC/ERM and Rho/ROCK/MLCP pathways in thrombin-induced formation of stress fibers and
523 increased endothelial permeability.

524 We next examined the role of ERM in thrombin-induced cytoskeletal changes. Thrombin
525 induces translocation of phosphorylated ERM from the cytoplasm to EC periphery during the
526 early stages of cells contraction and loss of monolayer integrity (Figure 11), which is consistent
527 with previous studies (1, 9, 35). Most importantly, our data again demonstrate differential roles
528 for the ERM proteins in response to thrombin. Moesin exerted a particularly prominent and

529 essential role in the promotion of EC barrier dysfunction by thrombin, while radixin appears to
530 have opposing effects. This observation is consistent with recent reports describing moesin
531 involvement in increased permeability induced by hypoxia and truncation of monocyte
532 chemoattractant protein 1 in the blood-brain barrier (25, 74) and AGE in human microvascular
533 EC (23, 68). Prior data obtained using knockout mice lacking individual ERM proteins largely
534 support the functional redundancy of the three ERM proteins (11, 32, 54). However recent
535 studies demonstrate differential biological functioning of these proteins. For example, ezrin and
536 moesin have distinct and critical functions in the T cell cortex during immunological synapse
537 formation (28). Moreover, ezrin, but not moesin, is phosphorylated on tyrosine in EGF-
538 challenged human A431 cells despite tyrosine 145 conservation in both proteins (17). In
539 addition, moesin has a non-redundant function in lymphocyte homeostasis (26). Our recent
540 findings also support the distinct biological roles of these proteins in agonist-mediated EC barrier
541 responses (1).

542 The observation that phosphorylated ERM is mostly localized to the peripheral area in EC
543 undergoing contraction after thrombin stimulation led us to examine the role of these proteins in
544 modulating permeability increases. We evaluated the role of ERM in thrombin-induced
545 hyperpermeability by measuring the TER in ERM depleted EC. The depletion of moesin alone or
546 triple ERM siRNA knockdown significantly attenuated the increase in permeability after
547 thrombin (Figure 8A, D and E). Ezrin knockdown also attenuated the decrease in TER induced
548 by thrombin, but to a lesser degree then moesin (Fig. 8C, E). In contrast, radixin depletion leads
549 to a slight increase in permeability during the early phase and delayed recovery during the later
550 phase of thrombin–mediated decreases in TER (Fig. 8B, E). These results suggest that ERM are
551 differentially involved in the development of thrombin-induced permeability with moesin and

552 ezrin promoting barrier permeability during the phase of active contraction (5-60 minutes of
553 treatment with thrombin). In contrast, despite the lower level of expression compare to moesin
554 and ezrin, radixin exerted a particularly prominent and essential role in the promotion of EC
555 barrier function in the restoration phase (60-120 minutes of treatment).

556 In EC, thrombin-induced activation of PAR_1 receptor initiate signaling through G_q- and
557 $G_{12/13}$-coupled Ca^{2+} mobilization, PKC and RhoA activation, and MAPK signaling (5, 7, 27). In
558 addition, thrombin transactivates PAR_2 through PAR_1 (48). We next used PAR_1 (TFLLR-NH_2),
559 PAR_2 (SLIGRL-NH_2) selective agonists and the PAR_1-specific blocking antibodies ATAP2 and
560 WEDE15 to determine the role of PARs in thrombin-induced threonine phosphorylation of
561 ERM. Our data indicate that thrombin primarily induces ERM threonine phosphorylation in
562 pulmonary EC by combined activation of both PAR_1 and PAR_2.

563

564 **Conclusion**

565 The present study demonstrates that thrombin induces PKC-dependent ERM
566 phosphorylation on a critical threonine residue (Ezrin-567, Radixin-564, Moesin-558) and
567 translocation of phosphorylated ERM to the EC periphery. ERM phosphorylation is mediated
568 by the combined actions of PAR_1 and PAR_2. Thrombin-induced barrier dysfunction in
569 pulmonary endothelium is associated with remodeling of the actin cytoskeleton that increases
570 permeability. ERM proteins are critically involved in the barrier-disruptive response induced in
571 the endothelium by thrombin and may modulate cytoskeletal changes and barrier
572 hyperpermeability via such intermediate signaling events as PKC mediated RhoA/ROCK-
573 dependent signaling. Our data demonstrate that depletion of either moesin alone, or of all three
574 ERM proteins, attenuates thrombin-induced F-actin cytoskeleton rearrangement, paracellular gap

formation, MLC phosphorylation and decrease in TER. In contrast, radixin depletion has the opposite effect on barrier function. Based on these results and our prior data (1), we propose the following model of ERM-dependent signaling in thrombin- and S1P-treated ECs (Fig. 14): thrombin treatment induces PAR_1 and PAR_2-mediated C-terminal threonine phosphorylation primarily of moesin and ezrin by PKC and PIP_2. Recently it has been reported that phosphorylation of the RhoA activator - guanine nucleotide exchange factor p115RhoGEF by PKC-α mediates TNF-α-induced RhoA activation and subsequent barrier dysfunction in mouse brain microvascular endothelial cells (51). We hypothesize that PKC isoforms may simultaneously phosphorylate both moesin and ezrin and p115RhoGEF. Activated moesin and ezrin may displace RhoGDI from RhoA, allowing p115RhoGEF mediated RhoA activation by GDP to GTP exchange. Increased intracellular concentration of Ca^{2+} activates MLCK. RhoA and MLCK phosphorylate MLC, allowing EC contraction and reorganization of the cytoskeleton, resulting in endothelial barrier dysfunction. In contrast, S1P induces S1PR1-mediated radixin activation (primarily), resulting in Rac1 activation. Activated Rac1 via its downstream target PAK1 induces actomyosin remodeling, including formation of a prominent cortical actin rim, which stabilizes cell-cell junctions, peripheral accumulation of phosphorylated MLC, and disappearance of central stress fibers, resulting in endothelial barrier enhancement. Thus, despite their structural similarities and reported functional redundancy, the ERM proteins differentially modulate thrombin-induced changes in lung EC cytoskeleton and permeability. These results advance our mechanistic understanding of EC barrier regulation, identify the ERM family as potential targets for therapeutic manipulation in this clinically important physiologic process and extend previous knowledge about the involvement of PKC and ERM in endothelial barrier regulation.

Acknowledgments

The authors are grateful to Drs. D. Fulton and S. Black from Georgia Health Sciences University for help with moesin mutant preparation.

Grants

This work was supported by grants from the National Institutes of Health (NIH) grant HL58064, HL88144 and HL101902.

References

1. **Adyshev DM, Moldobaeva NK, Elangovan VR, Garcia JG, and Dudek SM**. Differential involvement of ezrin/radixin/moesin proteins in sphingosine 1-phosphate-induced human pulmonary endothelial cell barrier enhancement. *Cellular signalling* 23: 2086-2096, 2011.
2. **Arpin M, Chirivino D, Naba A, and Zwaenepoel I**. Emerging role for ERM proteins in cell adhesion and migration. *Cell adhesion & migration* 5: 199-206, 2011.
3. **Belkina NV, Liu Y, Hao JJ, Karasuyama H, and Shaw S**. LOK is a major ERM kinase in resting lymphocytes and regulates cytoskeletal rearrangement through ERM phosphorylation. *Proceedings of the National Academy of Sciences of the United States of America* 106: 4707-4712, 2009.
4. **Berryman M, Franck Z, and Bretscher A**. Ezrin is concentrated in the apical microvilli of a wide variety of epithelial cells whereas moesin is found primarily in endothelial cells. *Journal of cell science* 105 (Pt 4): 1025-1043, 1993.
5. **Birukova AA, Birukov KG, Smurova K, Adyshev D, Kaibuchi K, Alieva I, Garcia JG, and Verin AD**. Novel role of microtubules in thrombin-induced endothelial barrier dysfunction. *Faseb J* 18: 1879-1890, 2004.
6. **Birukova AA, Smurova K, Birukov KG, Kaibuchi K, Garcia JG, and Verin AD**. Role of Rho GTPases in thrombin-induced lung vascular endothelial cells barrier dysfunction. *Microvascular research* 67: 64-77, 2004.
7. **Bogatcheva NV, Garcia JG, and Verin AD**. Molecular mechanisms of thrombin-induced endothelial cell permeability. *Biochemistry* 67: 75-84, 2002.
8. **Bogatcheva NV, and Verin AD**. The role of cytoskeleton in the regulation of vascular endothelial barrier function. *Microvascular research* 76: 202-207, 2008.
9. **Bogatcheva NV, Zemskova MA, Gorshkov BA, Kim KM, Daglis GA, Poirier C, and Verin AD**. Ezrin, radixin, and moesin are phosphorylated in response to 2-methoxyestradiol and modulate endothelial hyperpermeability. *American journal of respiratory cell and molecular biology* 45: 1185-1194, 2011.
10. **Cant SH, and Pitcher JA**. G protein-coupled receptor kinase 2-mediated phosphorylation of ezrin is required for G protein-coupled receptor-dependent reorganization of the actin cytoskeleton. *Molecular biology of the cell* 16: 3088-3099, 2005.
11. **Doi Y, Itoh M, Yonemura S, Ishihara S, Takano H, Noda T, and Tsukita S**. Normal development of mice and unimpaired cell adhesion/cell motility/actin-based cytoskeleton without compensatory up-regulation of ezrin or radixin in moesin gene knockout. *The Journal of biological chemistry* 274: 2315-2321, 1999.
12. **Dudek SM, and Garcia JG**. Cytoskeletal regulation of pulmonary vascular permeability. *Journal of Applied Physiology* 91: 1487-1500, 2001.
13. **Elbashir SM, Harborth J, Lendeckel W, Yalcin A, Weber K, and Tuschl T**. Duplexes of 21-nucleotide RNAs mediate RNA interference in cultured mammalian cells. *Nature* 411: 494-498, 2001.
14. **Fehon RG, McClatchey AI, and Bretscher A**. Organizing the cell cortex: the role of ERM proteins. *Nature reviews* 11: 276-287, 2010.
15. **Fievet BT, Gautreau A, Roy C, Del Maestro L, Mangeat P, Louvard D, and Arpin M**. Phosphoinositide binding and phosphorylation act sequentially in the activation mechanism of ezrin. *The Journal of cell biology* 164: 653-659, 2004.

16. **Fleegal MA, Hom S, Borg LK, and Davis TP**. Activation of PKC modulates blood-brain barrier endothelial cell permeability changes induced by hypoxia and posthypoxic reoxygenation. *Am J Physiol Heart Circ Physiol* 289: H2012-2019, 2005.
17. **Franck Z, Gary R, and Bretscher A**. Moesin, like ezrin, colocalizes with actin in the cortical cytoskeleton in cultured cells, but its expression is more variable. *Journal of cell science* 105 (Pt 1): 219-231, 1993.
18. **Garcia JG, Davis HW, and Patterson CE**. Regulation of endothelial cell gap formation and barrier dysfunction: role of myosin light chain phosphorylation. *Journal of cellular physiology* 163: 510-522, 1995.
19. **Garcia JG, Liu F, Verin AD, Birukova A, Dechert MA, Gerthoffer WT, Bamberg JR, and English D**. Sphingosine 1-phosphate promotes endothelial cell barrier integrity by Edg-dependent cytoskeletal rearrangement. *The Journal of clinical investigation* 108: 689-701, 2001.
20. **Garcia JG, Siflinger-Birnboim A, Bizios R, Del Vecchio PJ, Fenton JW, 2nd, and Malik AB**. Thrombin-induced increase in albumin permeability across the endothelium. *Journal of cellular physiology* 128: 96-104, 1986.
21. **Gautreau A, Louvard D, and Arpin M**. Morphogenic effects of ezrin require a phosphorylation-induced transition from oligomers to monomers at the plasma membrane. *The Journal of cell biology* 150: 193-203, 2000.
22. **Grand RJ, Turnell AS, and Grabham PW**. Cellular consequences of thrombin-receptor activation. *The Biochemical journal* 313 (Pt 2): 353-368, 1996.
23. **Guo X, Wang L, Chen B, Li Q, Wang J, Zhao M, Wu W, Zhu P, Huang X, and Huang Q**. ERM protein moesin is phosphorylated by advanced glycation end products and modulates endothelial permeability. *Am J Physiol Heart Circ Physiol* 297: H238-246, 2009.
24. **Hayashi K, Yonemura S, Matsui T, and Tsukita S**. Immunofluorescence detection of ezrin/radixin/moesin (ERM) proteins with their carboxyl-terminal threonine phosphorylated in cultured cells and tissues. *Journal of cell science* 112 (Pt 8): 1149-1158, 1999.
25. **Hicks K, O'Neil RG, Dubinsky WS, and Brown RC**. TRPC-mediated actin-myosin contraction is critical for BBB disruption following hypoxic stress. *American journal of physiology* 298: C1583-1593, 2010.
26. **Hirata T, Nomachi A, Tohya K, Miyasaka M, Tsukita S, Watanabe T, and Narumiya S**. Moesin-deficient mice reveal a non-redundant role for moesin in lymphocyte homeostasis. *International immunology* 24: 705-717, 2012.
27. **Holinstat M, Mehta D, Kozasa T, Minshall RD, and Malik AB**. Protein kinase Calpha-induced p115RhoGEF phosphorylation signals endothelial cytoskeletal rearrangement. *The Journal of biological chemistry* 278: 28793-28798, 2003.
28. **Ilani T, Khanna C, Zhou M, Veenstra TD, and Bretscher A**. Immune synapse formation requires ZAP-70 recruitment by ezrin and CD43 removal by moesin. *The Journal of cell biology* 179: 733-746, 2007.
29. **Ivetic A, and Ridley AJ**. Ezrin/radixin/moesin proteins and Rho GTPase signalling in leucocytes. *Immunology* 112: 165-176, 2004.
30. **Johnson MW, Miyata H, and Vinters HV**. Ezrin and moesin expression within the developing human cerebrum and tuberous sclerosis-associated cortical tubers. *Acta neuropathologica* 104: 188-196, 2002.
31. **Kim KM, Csortos C, Czikora I, Fulton D, Umapathy NS, Olah G, and Verin AD**. Molecular characterization of myosin phosphatase in endothelium. *Journal of cellular physiology* 227: 1701-1708, 2012.

32. **Kitajiri S, Fukumoto K, Hata M, Sasaki H, Katsuno T, Nakagawa T, Ito J, Tsukita S, and Tsukita S**. Radixin deficiency causes deafness associated with progressive degeneration of cochlear stereocilia. *The Journal of cell biology* 166: 559-570, 2004.
33. **Knezevic N, Roy A, Timblin B, Konstantoulaki M, Sharma T, Malik AB, and Mehta D**. GDI-1 phosphorylation switch at serine 96 induces RhoA activation and increased endothelial permeability. *Molecular and cellular biology* 27: 6323-6333, 2007.
34. **Konstantoulaki M, Kouklis P, and Malik AB**. Protein kinase C modifications of VE-cadherin, p120, and beta-catenin contribute to endothelial barrier dysregulation induced by thrombin. *Am J Physiol Lung Cell Mol Physiol* 285: L434-442, 2003.
35. **Koss M, Pfeiffer GR, 2nd, Wang Y, Thomas ST, Yerukhimovich M, Gaarde WA, Doerschuk CM, and Wang Q**. Ezrin/radixin/moesin proteins are phosphorylated by TNF-alpha and modulate permeability increases in human pulmonary microvascular endothelial cells. *J Immunol* 176: 1218-1227, 2006.
36. **Krieg J, and Hunter T**. Identification of the two major epidermal growth factor-induced tyrosine phosphorylation sites in the microvillar core protein ezrin. *The Journal of biological chemistry* 267: 19258-19265, 1992.
37. **Kumar P, Shen Q, Pivetti CD, Lee ES, Wu MH, and Yuan SY**. Molecular mechanisms of endothelial hyperpermeability: implications in inflammation. *Expert reviews in molecular medicine* 11: e19, 2009.
38. **Li Z, Liu YH, Xue YX, Liu LB, and Wang P**. Signal mechanisms underlying low-dose endothelial monocyte-activating polypeptide-II-induced opening of the blood-tumor barrier. *J Mol Neurosci* 48: 291-301, 2012 .
39. **Martiny-Baron G, Kazanietz MG, Mischak H, Blumberg PM, Kochs G, Hug H, Marme D, and Schachtele C**. Selective inhibition of protein kinase C isozymes by the indolocarbazole Go 6976. *The Journal of biological chemistry* 268: 9194-9197, 1993.
40. **Matsui T, Maeda M, Doi Y, Yonemura S, Amano M, Kaibuchi K, Tsukita S, and Tsukita S**. Rho-kinase phosphorylates COOH-terminal threonines of ezrin/radixin/moesin (ERM) proteins and regulates their head-to-tail association. *The Journal of cell biology* 140: 647-657, 1998.
41. **Matsui T, Yonemura S, Tsukita S, and Tsukita S**. Activation of ERM proteins in vivo by Rho involves phosphatidyl-inositol 4-phosphate 5-kinase and not ROCK kinases. *Curr Biol* 9: 1259-1262, 1999.
42. **McLaughlin JN, Shen L, Holinstat M, Brooks JD, Dibenedetto E, and Hamm HE**. Functional selectivity of G protein signaling by agonist peptides and thrombin for the protease-activated receptor-1. *The Journal of biological chemistry* 280: 25048-25059, 2005.
43. **Mehta D, and Malik AB**. Signaling mechanisms regulating endothelial permeability. *Physiological reviews* 86: 279-367, 2006.
44. **Minshall RD, Vandenbroucke EE, Holinstat M, Place AT, Tiruppathi C, Vogel SM, van Nieuw Amerongen GP, Mehta D, and Malik AB**. Role of protein kinase Czeta in thrombin-induced RhoA activation and inter-endothelial gap formation of human dermal microvessel endothelial cell monolayers. *Microvascular research* 80: 240-249, 2010.
45. **Moy AB, Blackwell K, and Kamath A**. Differential effects of histamine and thrombin on endothelial barrier function through actin-myosin tension. *Am J Physiol Heart Circ Physiol* 282: H21-29, 2002.
46. **Neisch AL, and Fehon RG**. Ezrin, Radixin and Moesin: key regulators of membrane-cortex interactions and signaling. *Current opinion in cell biology* 23: 377-382, 2011.

47. **Ng T, Parsons M, Hughes WE, Monypenny J, Zicha D, Gautreau A, Arpin M, Gschmeissner S, Verveer PJ, Bastiaens PI, and Parker PJ**. Ezrin is a downstream effector of trafficking PKC-integrin complexes involved in the control of cell motility. *The EMBO journal* 20: 2723-2741, 2001.

48. **O'Brien PJ, Prevost N, Molino M, Hollinger MK, Woolkalis MJ, Woulfe DS, and Brass LF**. Thrombin responses in human endothelial cells. Contributions from receptors other than PAR1 include the transactivation of PAR2 by thrombin-cleaved PAR1. *The Journal of biological chemistry* 275: 13502-13509, 2000.

49. **Patil SB, and Bitar KN**. RhoA- and PKC-alpha-mediated phosphorylation of MYPT and its association with HSP27 in colonic smooth muscle cells. *Am J Physiol Gastrointest Liver Physiol* 290: G83-95, 2006.

50. **Pearson MA, Reczek D, Bretscher A, and Karplus PA**. Structure of the ERM protein moesin reveals the FERM domain fold masked by an extended actin binding tail domain. *Cell* 101: 259-270, 2000.

51. **Peng J, He F, Zhang C, Deng X, and Yin F**. Protein kinase C-alpha signals P115RhoGEF phosphorylation and RhoA activation in TNF-alpha-induced mouse brain microvascular endothelial cell barrier dysfunction. *Journal of neuroinflammation* 8: 28, 2011.

52. **Pietromonaco SF, Simons PC, Altman A, and Elias L**. Protein kinase C-theta phosphorylation of moesin in the actin-binding sequence. *The Journal of biological chemistry* 273: 7594-7603, 1998.

53. **Rigor RR, Beard RS, Jr., Litovka OP, and Yuan SY**. Interleukin-1beta-induced barrier dysfunction is signaled through PKC-theta in human brain microvascular endothelium. *American journal of physiology* 302: C1513-1522, 2012.

54. **Saotome I, Curto M, and McClatchey AI**. Ezrin is essential for epithelial organization and villus morphogenesis in the developing intestine. *Developmental cell* 6: 855-864, 2004.

55. **Schaphorst KL, Pavalko FM, Patterson CE, and Garcia JG**. Thrombin-mediated focal adhesion plaque reorganization in endothelium: role of protein phosphorylation. *American journal of respiratory cell and molecular biology* 17: 443-455, 1997.

56. **Sonobe Y, Takeuchi H, Kataoka K, Li H, Jin S, Mimuro M, Hashizume Y, Sano Y, Kanda T, Mizuno T, and Suzumura A**. Interleukin-25 expressed by brain capillary endothelial cells maintains blood-brain barrier function in a protein kinase Cepsilon-dependent manner. *The Journal of biological chemistry* 284: 31834-31842, 2009.

57. **Srivastava J, Elliott BE, Louvard D, and Arpin M**. Src-dependent ezrin phosphorylation in adhesion-mediated signaling. *Molecular biology of the cell* 16: 1481-1490, 2005.

58. **Takahashi K, Sasaki T, Mammoto A, Takaishi K, Kameyama T, Tsukita S, and Takai Y**. Direct interaction of the Rho GDP dissociation inhibitor with ezrin/radixin/moesin initiates the activation of the Rho small G protein. *The Journal of biological chemistry* 272: 23371-23375, 1997.

59. **ten Klooster JP, Jansen M, Yuan J, Oorschot V, Begthel H, Di Giacomo V, Colland F, de Koning J, Maurice MM, Hornbeck P, and Clevers H**. Mst4 and Ezrin induce brush borders downstream of the Lkb1/Strad/Mo25 polarization complex. *Developmental cell* 16: 551-562, 2009.

60. **Tinsley JH, De Lanerolle P, Wilson E, Ma W, and Yuan SY**. Myosin light chain kinase transference induces myosin light chain activation and endothelial hyperpermeability. *American journal of physiology* 279: C1285-1289, 2000.

61. **Tinsley JH, Teasdale NR, and Yuan SY**. Involvement of PKCdelta and PKD in pulmonary microvascular endothelial cell hyperpermeability. *American journal of physiology* 286: C105-111, 2004.
62. **Titchenell PM, Lin CM, Keil JM, Sundstrom JM, Smith CD, and Antonetti DA**. Novel atypical PKC inhibitors prevent vascular endothelial growth factor-induced blood-retinal barrier dysfunction. *The Biochemical journal* 446: 455-467, 2012.
63. **Toullec D, Pianetti P, Coste H, Bellevergue P, Grand-Perret T, Ajakane M, Baudet V, Boissin P, Boursier E, Loriolle F, and et al.** The bisindolylmaleimide GF 109203X is a potent and selective inhibitor of protein kinase C. *The Journal of biological chemistry* 266: 15771-15781, 1991.
64. **van Nieuw Amerongen GP, van Delft S, Vermeer MA, Collard JG, and van Hinsbergh VW**. Activation of RhoA by thrombin in endothelial hyperpermeability: role of Rho kinase and protein tyrosine kinases. *Circulation research* 87: 335-340, 2000.
65. **Verin AD, Birukova A, Wang P, Liu F, Becker P, Birukov K, and Garcia JG**. Microtubule disassembly increases endothelial cell barrier dysfunction: role of MLC phosphorylation. *Am J Physiol Lung Cell Mol Physiol* 281: L565-574, 2001.
66. **Vu TK, Hung DT, Wheaton VI, and Coughlin SR**. Molecular cloning of a functional thrombin receptor reveals a novel proteolytic mechanism of receptor activation. *Cell* 64: 1057-1068, 1991.
67. **Wald FA, Oriolo AS, Mashukova A, Fregien NL, Langshaw AH, and Salas PJ**. Atypical protein kinase C (iota) activates ezrin in the apical domain of intestinal epithelial cells. *Journal of cell science* 121: 644-654, 2008.
68. **Wang J, Liu H, Chen B, Li Q, Huang X, Wang L, Guo X, and Huang Q**. RhoA/ROCK-dependent moesin phosphorylation regulates AGE-induced endothelial cellular response. *Cardiovascular diabetology* 11: 7, 2012.
69. **Wilkinson SE, Parker PJ, and Nixon JS**. Isoenzyme specificity of bisindolylmaleimides, selective inhibitors of protein kinase C. *The Biochemical journal* 294 (Pt 2): 335-337, 1993.
70. **Willis CL, Meske DS, and Davis TP**. Protein kinase C activation modulates reversible increase in cortical blood-brain barrier permeability and tight junction protein expression during hypoxia and posthypoxic reoxygenation. *J Cereb Blood Flow Metab* 30: 1847-1859, 2010.
71. **Wu KL, Khan S, Lakhe-Reddy S, Jarad G, Mukherjee A, Obejero-Paz CA, Konieczkowski M, Sedor JR, and Schelling JR**. The NHE1 Na+/H+ exchanger recruits ezrin/radixin/moesin proteins to regulate Akt-dependent cell survival. *The Journal of biological chemistry* 279: 26280-26286, 2004.
72. **Wysolmerski RB, and Lagunoff D**. Regulation of permeabilized endothelial cell retraction by myosin phosphorylation. *The American journal of physiology* 261: C32-40, 1991.
73. **Yang HS, and Hinds PW**. Increased ezrin expression and activation by CDK5 coincident with acquisition of the senescent phenotype. *Molecular cell* 11: 1163-1176, 2003.
74. **Yao Y, and Tsirka SE**. Truncation of monocyte chemoattractant protein 1 by plasmin promotes blood-brain barrier disruption. *Journal of cell science* 124: 1486-1495, 2011.

851 **Figure Legends**

852 **Figure 1. Relative quantity of moesin (MSN), ezrin (EZR), and radixin (RDX) mRNA in**
853 **HPAEC.** Total RNA was isolated from human pulmonary artery endothelial cells (HPAEC) and
854 quantitative real-time reverse transcriptase-polymerase chain reaction (qRT-PCR) was performed
855 using target gene specific primers and probes and the relative amounts expressed using standard
856 curve method as described in Methods. Each value represents the mean of triplicates.
857
858 **Figure 2. Time-dependent effects of thrombin on threonine phosphorylation of ERM.** (A)
859 Confluent HPAEC were treated either with control vehicle or thrombin (0.5 U/ml) for the
860 indicated times, and phosphorylated ERM (phospho-Ezrin (Thr567)/Radixin (Thr564)/Moesin
861 (Thr558) was detected via immunoblotting. (B) The bar graph represents relative densitometry.
862 Data are presented as fold changes in phosphorylated ERM over vehicle-treated control and
863 expressed as means ± S.E. from three independent experiments. **P* < 0.05 vs. unstimulated
864 control.
865
866 **Figure 3. Thrombin-induced ERM phosphorylation requires activation of PKC.** HPAEC
867 were pretreated with either control vehicle or the following inhibitors: PKC inhibitors Ro-31-
868 7549 (10 μM, A, C) for 30 min, bisindolylmaleimide (BIM, 1 μM, C) for 30 min, Go6976 (1
869 μM, C) for 1 h, Ca(2+) chelator BAPTA-AM (25 μM, A) for 1 h, p38 kinase inhibitor
870 SB203580 (20 μM, A, B) for 30 min, Rho kinase inhibitors Y-27632 (10 μM, A, B) for 1 h and
871 H-1152 (3 μM, B) for 1 h, PI3 Kinase inhibitor LY294002 (10 μM, A) for 1 hr. EC were then
872 stimulated with EBM-2 medium alone or thrombin (0.5 U/ml) for the indicated time.
873 Phosphorylation of ERM proteins and MLC were analyzed by immunoblotting of cell lysates

874 with phospho-ERM (as in Fig. 2) or di-phospho-MLC (Thr18/Ser19) specific Abs. GAPDH or β-
875 actin Abs were used as a normalization control. Rearranged lanes from the same blot are outlined
876 by vertical dotted line. Results of scanning densitometry of Western blots are shown as fold
877 changes of ERM or MLC phosphorylation relative to vehicle treated EC stimulated by thrombin.
878 Results are representative of 3-6 independent experiments. Values are means ± S.E. *,
879 significantly different from cells treated with vehicle ($p < 0.05$); **, significantly different from
880 cells stimulated with thrombin ($p < 0.05$).
881
882 **Figure 4. Effects of thrombin on phosphorylation of PKC isoforms in HPAEC.** Confluent
883 HPAEC were treated either with control vehicle or thrombin (0.5U/ml) for the indicated times,
884 and phosphorylated PKCβ (A), PKCγ (B), PKCε (C), PKCζ (D), PKCθ (E), and PKCδ (F) were
885 detected via immunoblotting. Bar graphs represent relative densitometry of fold changes in
886 phosphorylated PKC isoforms after thrombin relative to vehicle-treated control and expressed as
887 means ± S.E. from three independent experiments. *, significantly different from cells treated
888 with EBM-2 ($p < 0.05$); #, significantly different from cells treated with EBM-2 ($p < 0.01$).
889
890 **Figure 5. Depletion of PKC isoforms by siRNA.** PKCε (A) and PKCγ (B) depletion were
891 induced by specific siRNA duplexes and assessed for silencing effects by immunoblotting with
892 appropriate Ab, as compared with treatment with nonspecific (ns) siRNA. Immunoblotting with
893 β-actin Ab was used as a normalization control. Rearranged lanes from the same blot are outlined
894 by vertical dotted line. Quantitative analysis of protein expression was performed by scanning
895 densitometry and expressed in relative density units (RDU). Results are means ± S.E. for three

896 independent experiments. #, significant difference ($p < 0.01$) when compared with cells treated
897 with ns siRNA.
898
899 **Figure 6. Depletion of PKC isoforms inhibits thrombin-induced ERM and MLC**
900 **phosphorylation.** Confluent HPAEC were incubated with non-specific, PKCβI-, PKCζ-, PKCθ-
901 , PKCδ-, PKCγ- and PKCε- specific siRNA (A) or with non-specific, combinations of PKCδ-
902 and PKCε-, combinations of PKCγ- , PKCδ- and PKCε- and combinations of PKCβI - , PKCθ-
903 and PKCζ- specific siRNAs (C) as described in Methods, and then stimulated by thrombin (0.5
904 U/ml, 5 min) or vehicle. Total lysates were analyzed by immunoblotting for phospho-ERM or di-
905 phospho-MLC (Thr18/Ser19). Immunoblotting with β-tubulin Ab was used as a normalization
906 control. Rearranged lanes from the same blot are outlined by vertical dotted line. (B, D, E) The
907 bar graphs represent relative densitometry of fold changes in phosphorylated ERM and MLC
908 after thrombin relative to vehicle-treated control. Results are means ± S.E. of four independent
909 experiments. *, significantly different from cells treated with ns siRNA without thrombin ($p <$
910 0.01); #, significantly different from cells treated with ns siRNA without thrombin ($p < 0.05$). **,
911 significantly different from cells treated with ns siRNA and thrombin ($p < 0.05$).
912
913 **Figure 7. Effects of ERM depletion on thrombin-induced ERM and MLC phosphorylation.**
914 Confluent HPAEC were incubated with non-specific, moesin- (panel A), radixin- (panel B),
915 ezrin-specific (panel C) or combined siRNAs for ezrin, radixin, and moesin (panel D) as
916 described in Methods then stimulated by thrombin (0.5 U/ml, 5 min) or vehicle. Total lysates
917 were analyzed by immunoblotting with phospho-ERM or di-phospho-MLC (Thr18/Ser19) Abs.
918 Immunoblotting with β-tubulin Ab was used as a normalization control. The bar graphs

919 represents relative densitometry of fold changes in phosphorylated ERM and MLC after
920 thrombin relative to vehicle-treated control. Results are means ± S.E. of three independent
921 experiments. *p<0.05, compared with corresponding pretreatment vehicle control.

922 **Figure 8. Effects of ERM depletion on thrombin-induced endothelial barrier**
923 **hyperpermeability.** EC grown in chambers on gold microelectrodes were transfected with
924 siRNA for moesin (panel A), radixin (panel B), ezrin (panel C), combined siRNAs for ezrin,
925 radixin, and moesin (panel D), or treated with nonspecific (ns) siRNA, as described in Methods
926 and used for transendothelial electrical resistance (TER) measurements. At time = 0, cells were
927 stimulated with thrombin (0.5 U/ml) or vehicle control. Shown are pooled data of 5 independent
928 experiments. The bar graph (E) depicts pooled TER data (n = 5) as maximal value of normalized
929 TER elevation above base line achieved within 30 min ± S.E. *, significantly different from cells
930 treated with ns siRNA reagent without thrombin ($p < 0.05$); **, significantly different from
931 control cells stimulated with thrombin ($p < 0.05$).

932

933 **Figure 9. Effects of PAR_1 blocking antibodies on thrombin-induced ERM phosphorylation.**
934 (A) HPAEC were pretreated for 1 hour with either control vehicle or the PAR_1 blocking Abs
935 ATAP2 (25 μg/ml) or WEDE15 (25 μg/ml) or with combination of ATAP2 and WEDE15, then
936 stimulated by thrombin (0.5 U/ml, 5 min) or vehicle. Total lysates were analyzed by
937 immunoblotting for phospho-ERM. Immunoblotting with β-actin Ab was used as a
938 normalization control. (B) The bar graph represents relative densitometry of fold changes in
939 phosphorylated ERM after thrombin relative to vehicle-treated control. Results are means ± S.E.
940 of four independent experiments. *, significantly different from cells treated with ns siRNA
941 without S1P ($p < 0.05$); #, significantly different from cells treated with ns siRNA without

thrombin ($p < 0.01$). **, significantly different from cells treated with ns siRNA and thrombin ($p < 0.05$).

Figure 10. Effects of PAR_1 and PAR_2 selective agonists on thrombin-induced ERM phosphorylation. (A) EC were pretreated for 5 minutes with thrombin (0.5 U/ml), PAR_1 selective agonist TFLLR-NH_2 (50 μM), PAR_2 selective agonist SLIGRL-NH_2 (50 μM) or combination of TFLLR-NH_2 and SLIGRL-NH_2. Pretreatment with vehicle and reversed amino acid sequence peptides RLLFT-NH_2 and LRGILS-NH_2 used as controls. (B) The bar graph represents relative densitometry of fold changes in phosphorylated ERM after thrombin, TFLLR-NH_2 or SLIGRL-NH_2 relative to vehicle-treated control. Results are means ± S.E. of three independent experiments. *p<0.05, compared with corresponding pretreatment controls.

Figure 11. Distribution of phospho-ERM in EC after thrombin. EC grown on glass cover slips and treated with 0.5 U/ml thrombin for indicated time (images b-e) or non treated control cells (image a) were subjected to immunofluorescent staining with anti-phospho-ERM Ab. The phospho- ERM signal is very weak in quiescent monolayers and is evident only in spike-like structures in cell-cell border areas (image a, arrow 1). Threonine-phosphorylated ERM proteins predominantly localized to the periphery of ECs following thrombin stimulation (5-15 min, images b,c, arrow 2) and also are detectable in peripheral spike-like structures (image b, arrow 1). After 1-2 hrs phosphorylated ERM localized in spike-like structures characteristic of quiescent cells and in cytoplasm (images d,e). Images are representative of 3 independent experiments. Scale bar = 10 μm.

Figure 12. Effects of ERM depletion on thrombin-induced cytoskeletal remodeling. HPAEC grown on glass cover slips were incubated with siRNA to ezrin, radixin, moesin, or combination of siRNAs to all three proteins, or treated with non-specific siRNA duplex as described in Methods followed by thrombin treatment (0.5 U/ml, 5 min). ECs were subjected to double immunofluorescent staining with Texas Red phalloidin to visualize F-actin (panels A and B, upper images) and anti-pp-MLC Ab (Panels A and B, bottom images). Incubation with siRNA to moesin (g, h) and combined siRNAs to ezrin, radixin, and moesin (o, p) almost completely abolishes thrombin-induced F-actin stress fiber and gap formation and MLC phosphorylation compared with control (nsRNA) incubation (c, d, arrows). In contrast, pretreatment with siRNA to radixin slightly *enhances* the thickness of stress fibers and MLC phosphorylation (k, l, arrows) compared with incubation with nsRNA. Bar = 10 μM. Images are representative of three independent experiments.

Figure 13. Effects of overexpression of the phosphorylation-deficient mutant of moesin (Thr558Ala) on thrombin-induced cytoskeletal remodeling. (A) ECs were transfected with empty vector (control), V5 tagged wild-type or mutant moesin, which were then detected via immunoblotting with V5 Ab. Results of scanning densitometry of Western blots are shown as % of moesin relative to control. Immunoblotting with β-actin Ab was used as a normalization control. (B) After transfection with vectors expressing moesin (wild-type or mutant) tagged with V5, EC were grown on glass cover slips as described in Methods followed by thrombin treatment (0.5 U/ml, 5 min). ECs were subjected to double immunofluorescent staining with Texas Red phalloidin to visualize F-actin (panels B and C, upper images) and V5 Ab (Panels B and C, bottom images). Overexpression with mutant moesin abolishes thrombin-induced F-actin stress

fibers and induces cortical actin formation (panel C, image g) compared to EC overexpressed with wild type moesin (panel C, image c). Arrow indicates cell transfected with mutant moesin EC (panel C, image g). Images are representative of three independent experiments. Scale bar = 10 μm.

Figure 14. Proposed model of ERM-dependent signaling in thrombin- and S1P-challenged lung endothelium (see explanation in Conclusion).

Figure 1

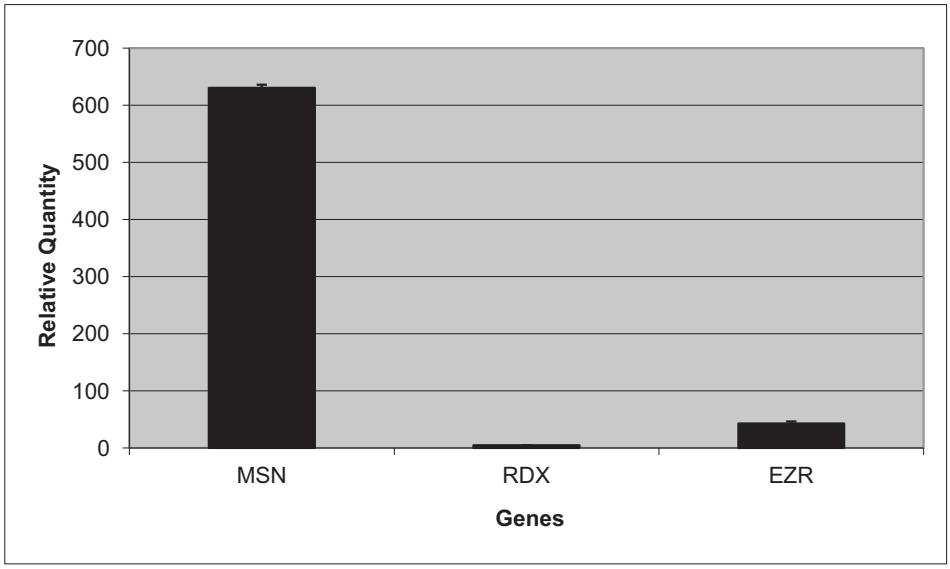
700
600
500
400
300
200
100
0
Relative Quantity
MSN
RDX
EZR
Genes

Figure 2

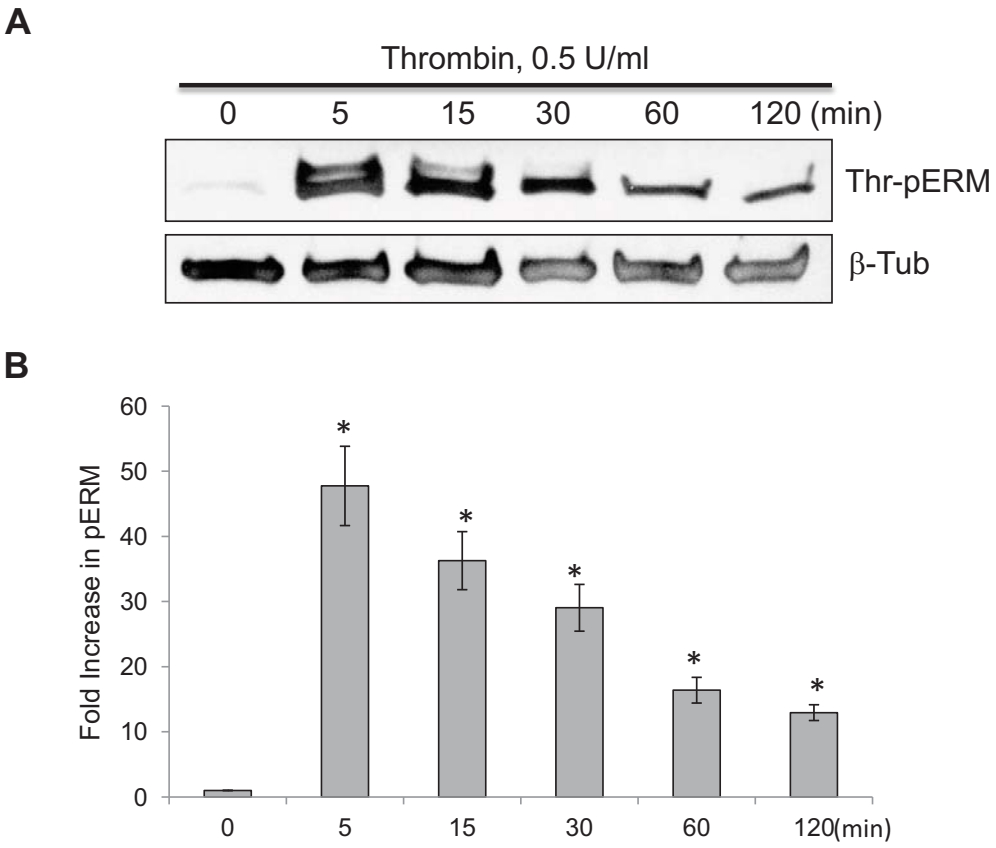
A
Thrombin, 0.5 U/ml
0
5
15
30
60
120 (min)
Thr-pERM
β-Tub
B
Fold Increase in pERM
60
50
40
30
20
10
0
*
0
5
15
30
60
120(min)

Figure 3A

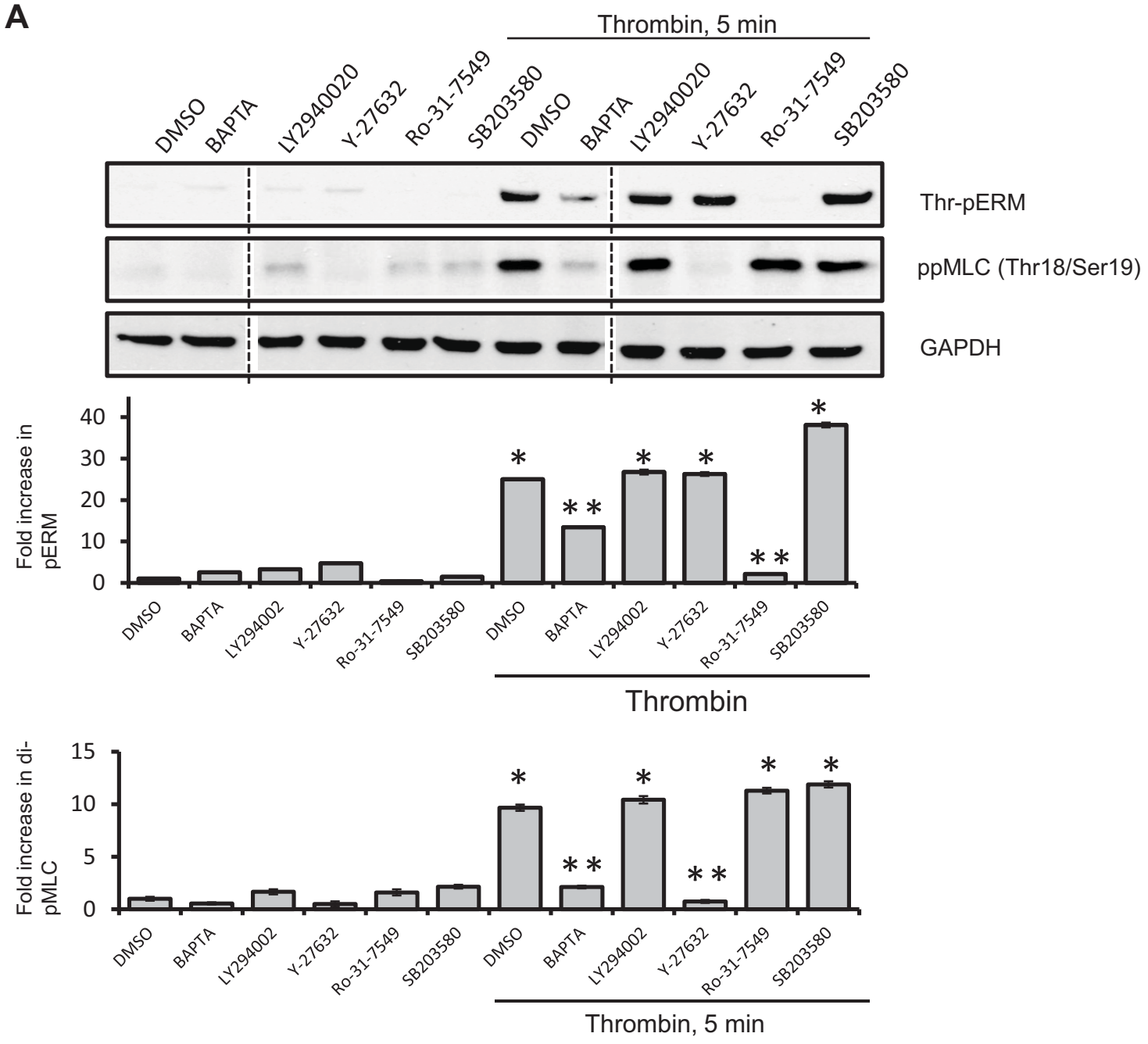
A
Thrombin, 5 min
DMSO
BAPTA
LY2940020
Y-27632
Ro-31-7549
SB203580
DMSO
BAPTA
LY2940020
Y-27632
Ro-31-7549
SB203580
Thr-pERM
ppMLC (Thr18/Ser19)
GAPDH
Fold increase in pERM
40
30
20
10
0
DMSO
BAPTA
LY294002
Y-27632
Ro-31-7549
SB203580
DMSO
BAPTA
LY294002
Y-27632
Ro-31-7549
SB203580
Thrombin
Fold increase in di-pMLC
15
10
5
0
DMSO
BAPTA
LY294002
Y-27632
Ro-31-7549
SB203580
DMSO
BAPTA
LY294002
Y-27632
Ro-31-7549
SB203580
Thrombin, 5 min

Figure 3B

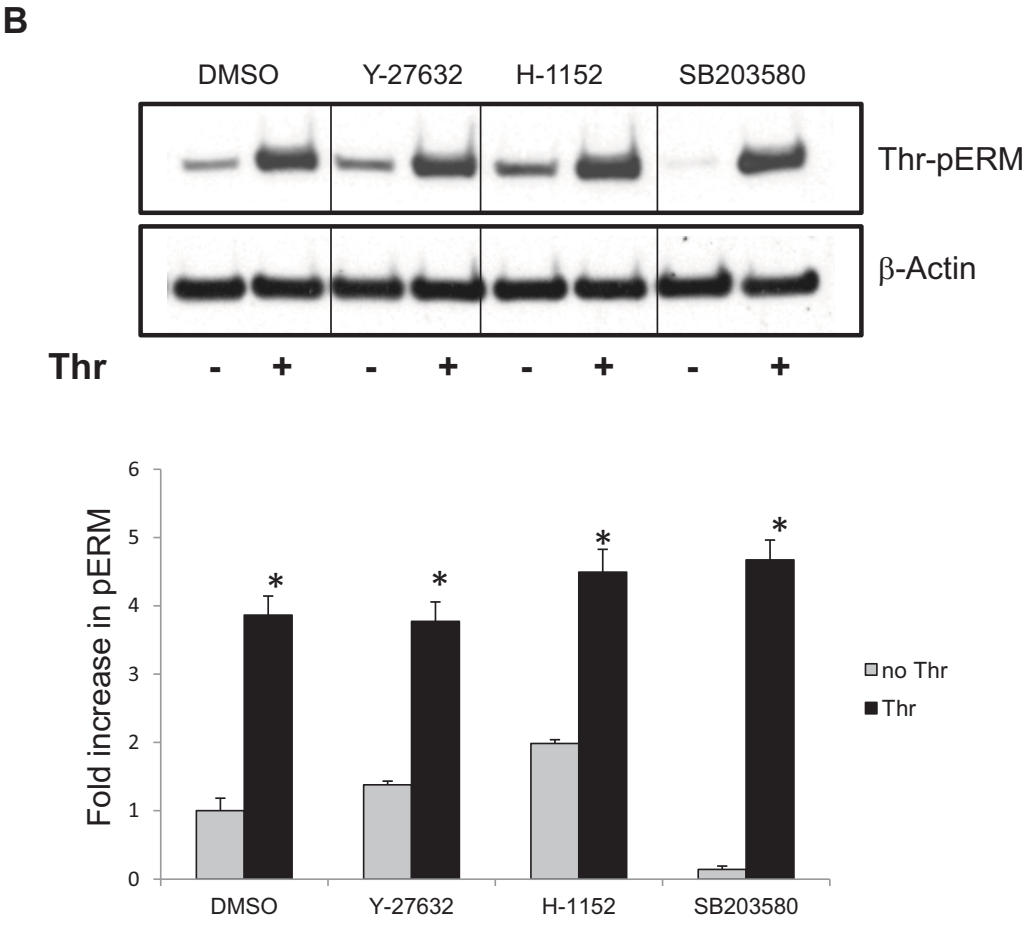
B
DMSO
Y-27632
H-1152
SB203580
Thr-pERM
β-Actin
Thr
- + - + - + - +
Fold increase in pERM
0
1
2
3
4
5
6
*
*
*
*
DMSO
Y-27632
H-1152
SB203580
no Thr
Thr

Figure 3C

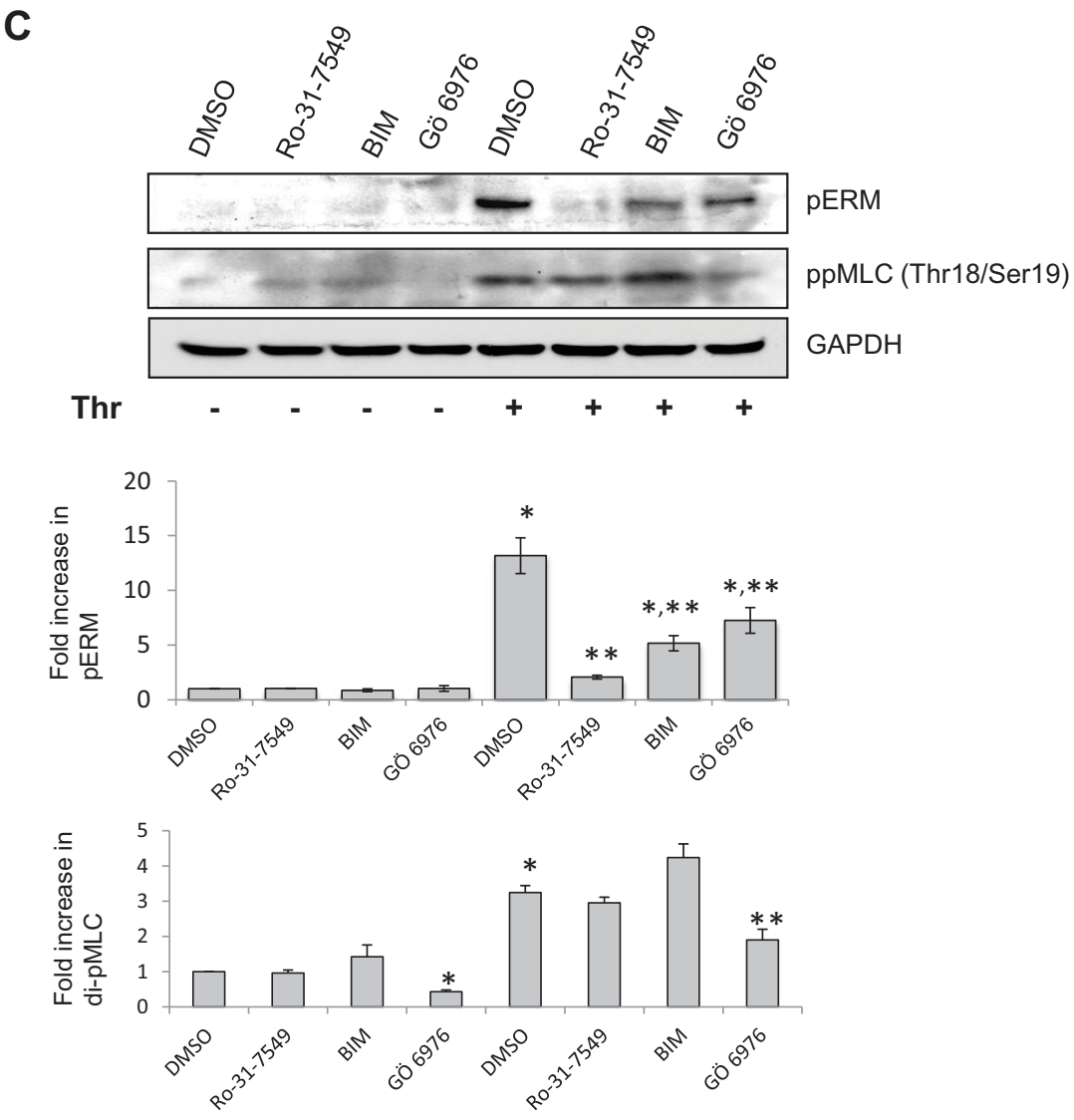
C
DMSO
Ro-31-7549
BIM
Gö 6976
DMSO
Ro-31-7549
BIM
Gö 6976
pERM
ppMLC (Thr18/Ser19)
GAPDH
Thr - - - - + + + +
Fold increase in pERM
20
15
10
5
0
*
**
*,**
*,**
DMSO
Ro-31-7549
BIM
GÖ 6976
DMSO
Ro-31-7549
BIM
GÖ 6976
Fold increase in di-pMLC
5
4
3
2
1
0
*
*
**
DMSO
Ro-31-7549
BIM
GÖ 6976
DMSO
Ro-31-7549
BIM
GÖ 6976

Figure 4A-D

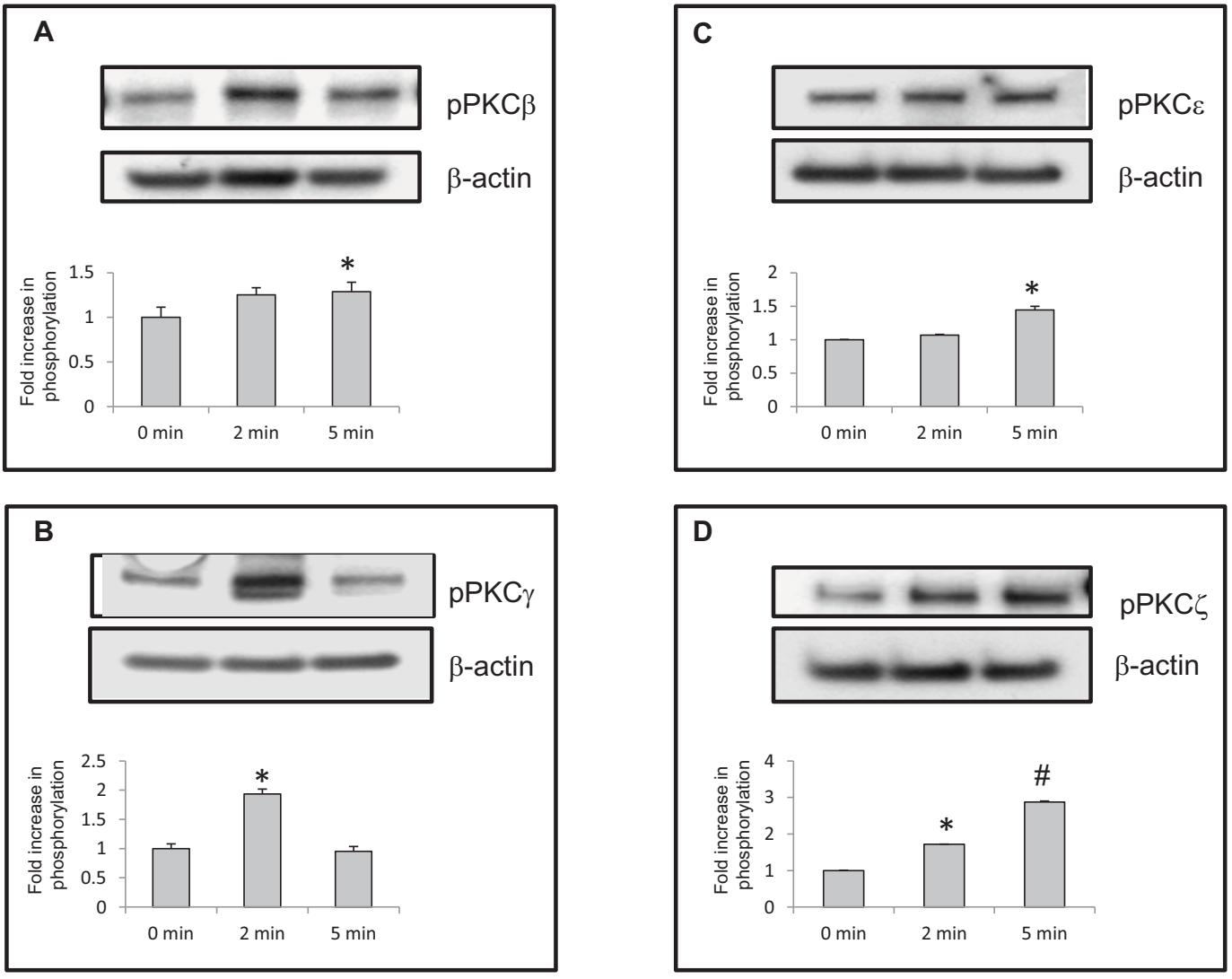
A
pPKCβ
β-actin
Fold increase in phosphorylation
1.5
1
0.5
0
*
0 min
2 min
5 min
C
pPKCε
β-actin
Fold increase in phosphorylation
2
1.5
1
0.5
0
*
0 min
2 min
5 min
B
pPKCγ
β-actin
Fold increase in phosphorylation
2.5
2
1.5
1
0.5
0
*
0 min
2 min
5 min
D
pPKCζ
β-actin
Fold increase in phosphorylation
4
3
2
1
0
*
#
0 min
2 min
5 min

Figure 4E, F

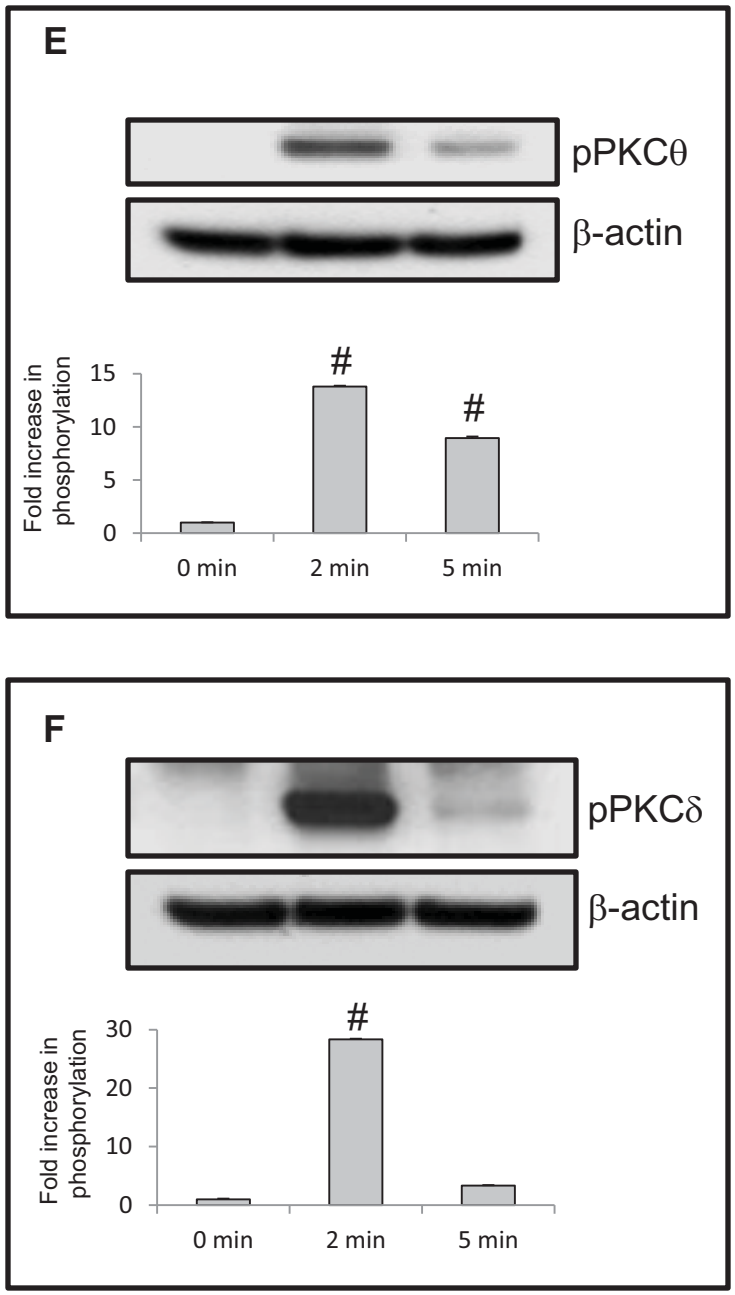
E
pPKCθ
β-actin
Fold increase in phosphorylation
15
10
5
0
#
#
0 min
2 min
5 min
F
pPKCδ
β-actin
Fold increase in phosphorylation
30
20
10
0
#
0 min
2 min
5 min

Figure 5

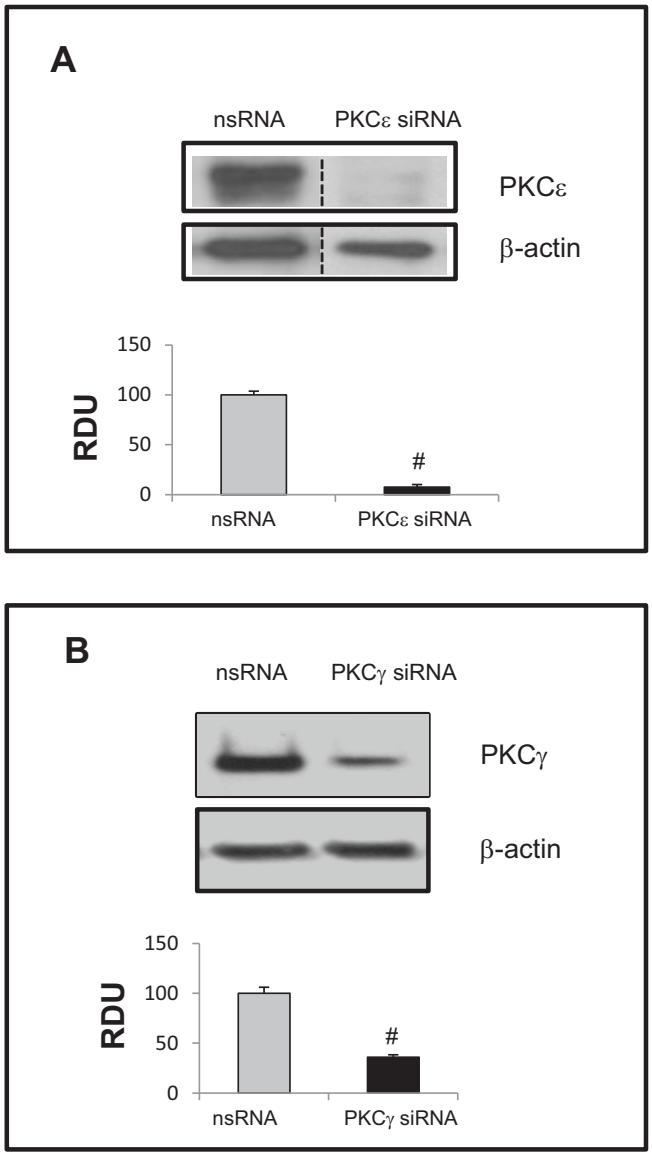
A
nsRNA
PKCε siRNA
PKCε
β-actin
RDU
150
100
50
0
#
nsRNA
PKCε siRNA
B
nsRNA
PKCγ siRNA
PKCγ
β-actin
RDU
150
100
50
0
#
nsRNA
PKCγ siRNA

Figure 6A, B

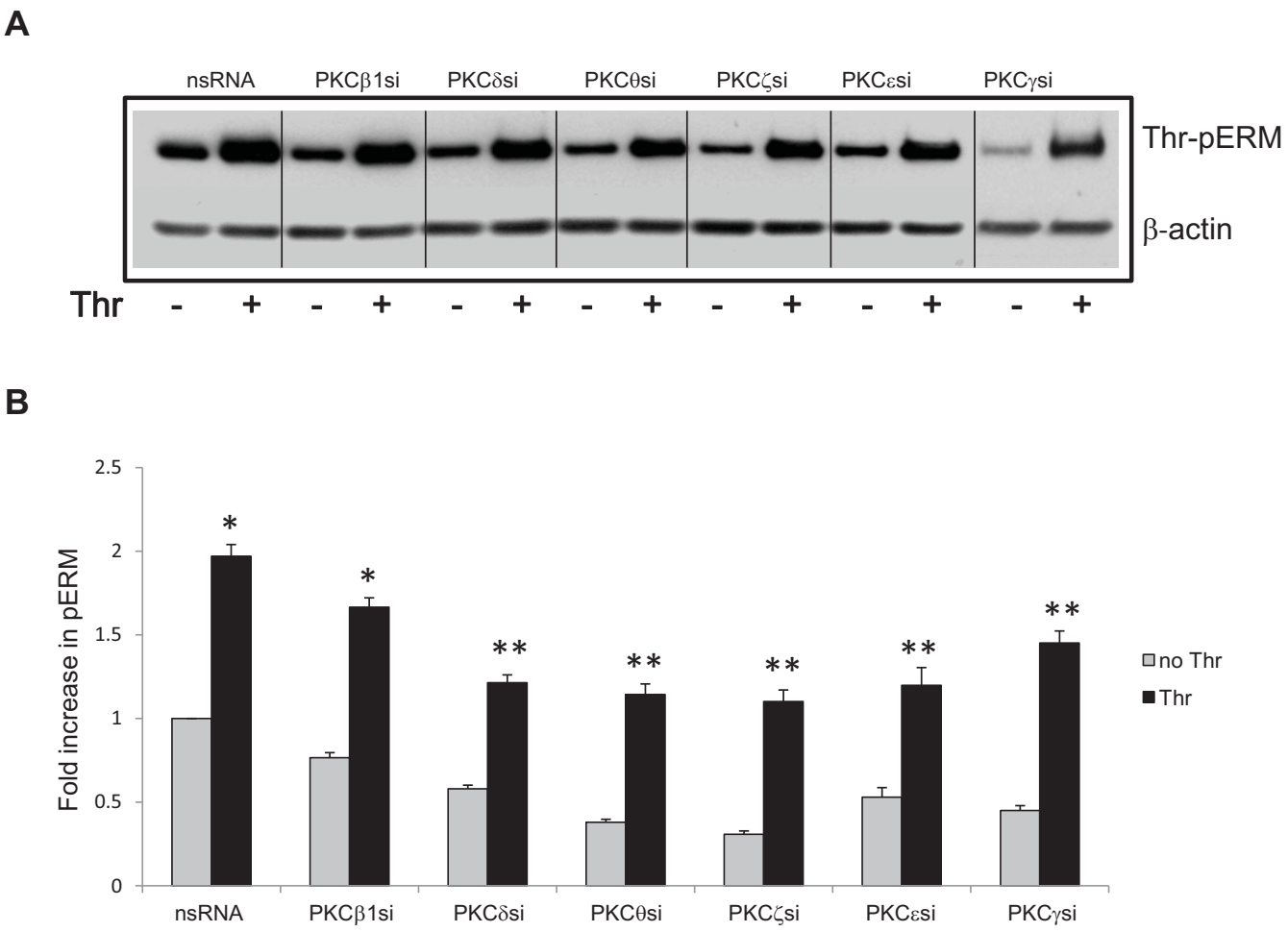
A
nsRNA
PKCβ1si
PKCδsi
PKCθsi
PKCζsi
PKCεsi
PKCγsi
Thr-pERM
β-actin
Thr - + - + - + - + - + - + - +
B
Fold increase in pERM
2.5
2
1.5
1
0.5
0
*
*
**
**
**
**
**
nsRNA
PKCβ1si
PKCδsi
PKCθsi
PKCζsi
PKCεsi
PKCγsi
no Thr
Thr

Figure 6C, D, E

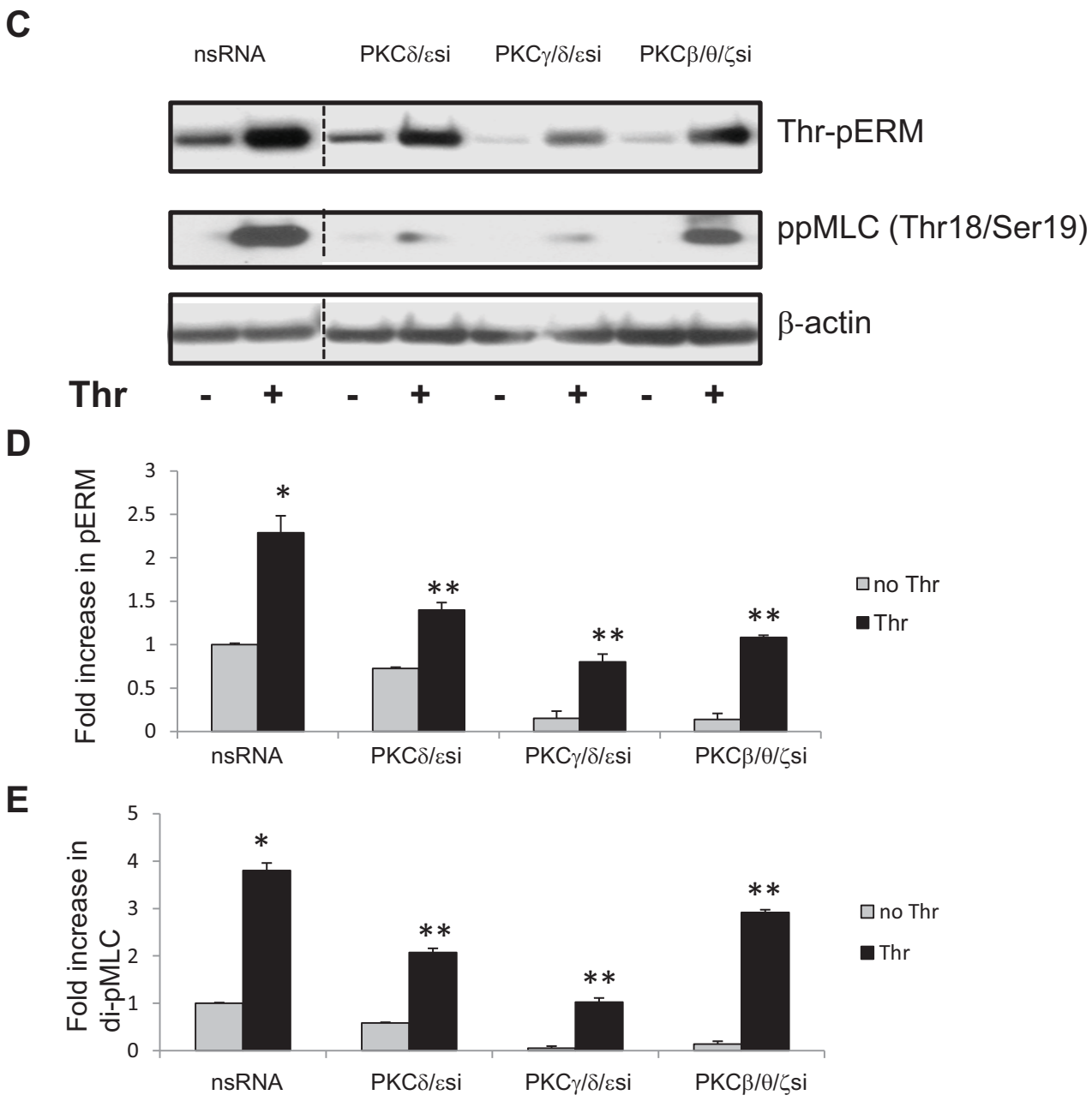
C
nsRNA
PKCδ/εsi
PKCγ/δ/εsi
PKCβ/θ/ζsi
Thr-pERM
ppMLC (Thr18/Ser19)
β-actin
Thr - + - + - + - +
D
Fold increase in pERM
3
2.5
2
1.5
1
0.5
0
*
**
**
**
nsRNA
PKCδ/εsi
PKCγ/δ/εsi
PKCβ/θ/ζsi
no Thr
Thr
E
Fold increase in di-pMLC
5
4
3
2
1
0
*
**
**
**
nsRNA
PKCδ/εsi
PKCγ/δ/εsi
PKCβ/θ/ζsi
no Thr
Thr

Figure 7A, B

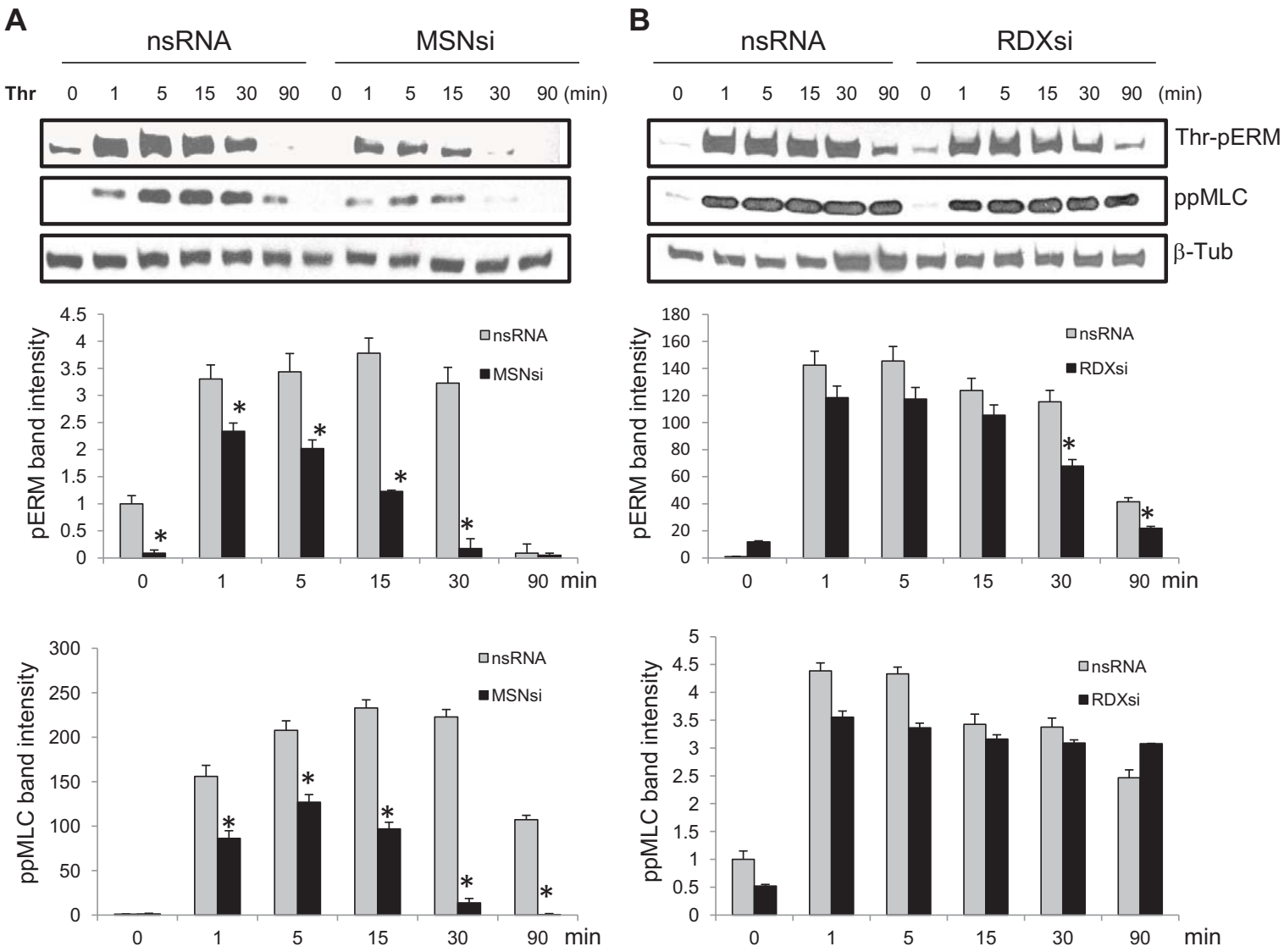
A
nsRNA
MSNsi
Thr 0 1 5 15 30 90 0 1 5 15 30 90 (min)
pERM band intensity
nsRNA
MSNsi
0 1 5 15 30 90 min
ppMLC band intensity
nsRNA
MSNsi
0 1 5 15 30 90 min
B
nsRNA
RDXsi
0 1 5 15 30 90 0 1 5 15 30 90 (min)
Thr-pERM
ppMLC
β-Tub
pERM band intensity
nsRNA
RDXsi
0 1 5 15 30 90 min
ppMLC band intensity
nsRNA
RDXsi
0 1 5 15 30 90 min

Figure 7C, D

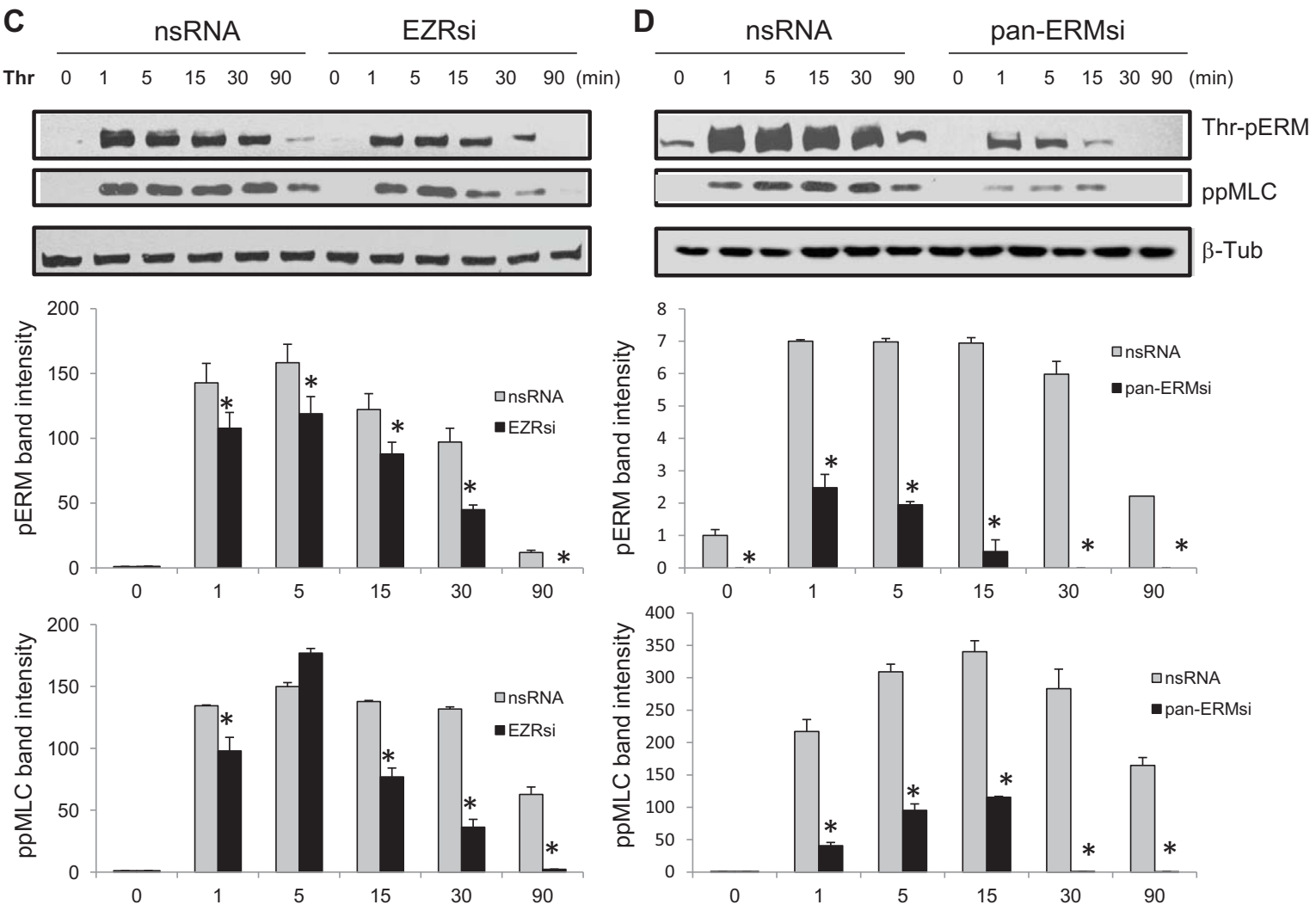
C
nsRNA
EZRsi
Thr 0 1 5 15 30 90 0 1 5 15 30 90 (min)
Thr-pERM
ppMLC
β-Tub
pERM band intensity
ppMLC band intensity
nsRNA
EZRsi
D
nsRNA
pan-ERMsi
0 1 5 15 30 90 0 1 5 15 30 90 (min)
Thr-pERM
ppMLC
β-Tub
pERM band intensity
ppMLC band intensity
nsRNA
pan-ERMsi

Figure 8A, B

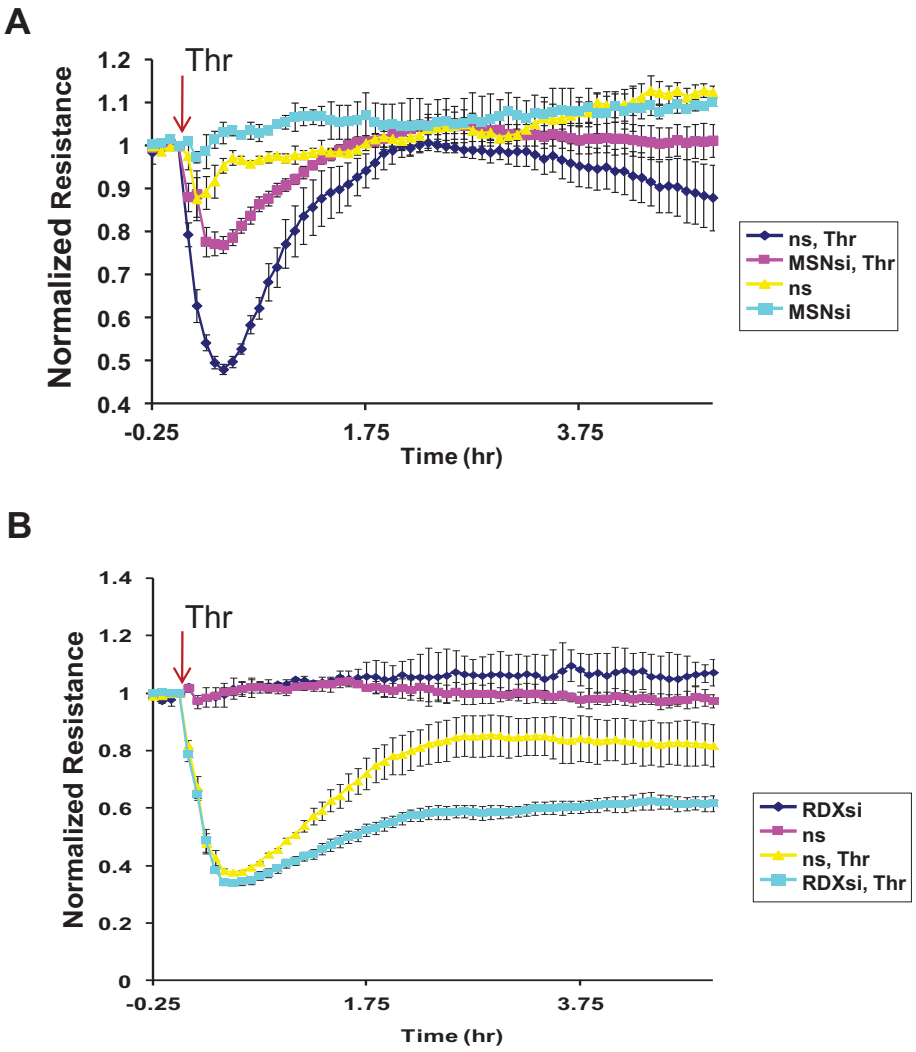
A
Thr
Normalized Resistance
1.2
1.1
1
0.9
0.8
0.7
0.6
0.5
0.4
-0.25
1.75
3.75
Time (hr)
ns, Thr
MSNsi, Thr
ns
MSNsi
B
Thr
Normalized Resistance
1.4
1.2
1
0.8
0.6
0.4
0.2
0
-0.25
1.75
3.75
Time (hr)
RDXsi
ns
ns, Thr
RDXsi, Thr

Figure 8C, D

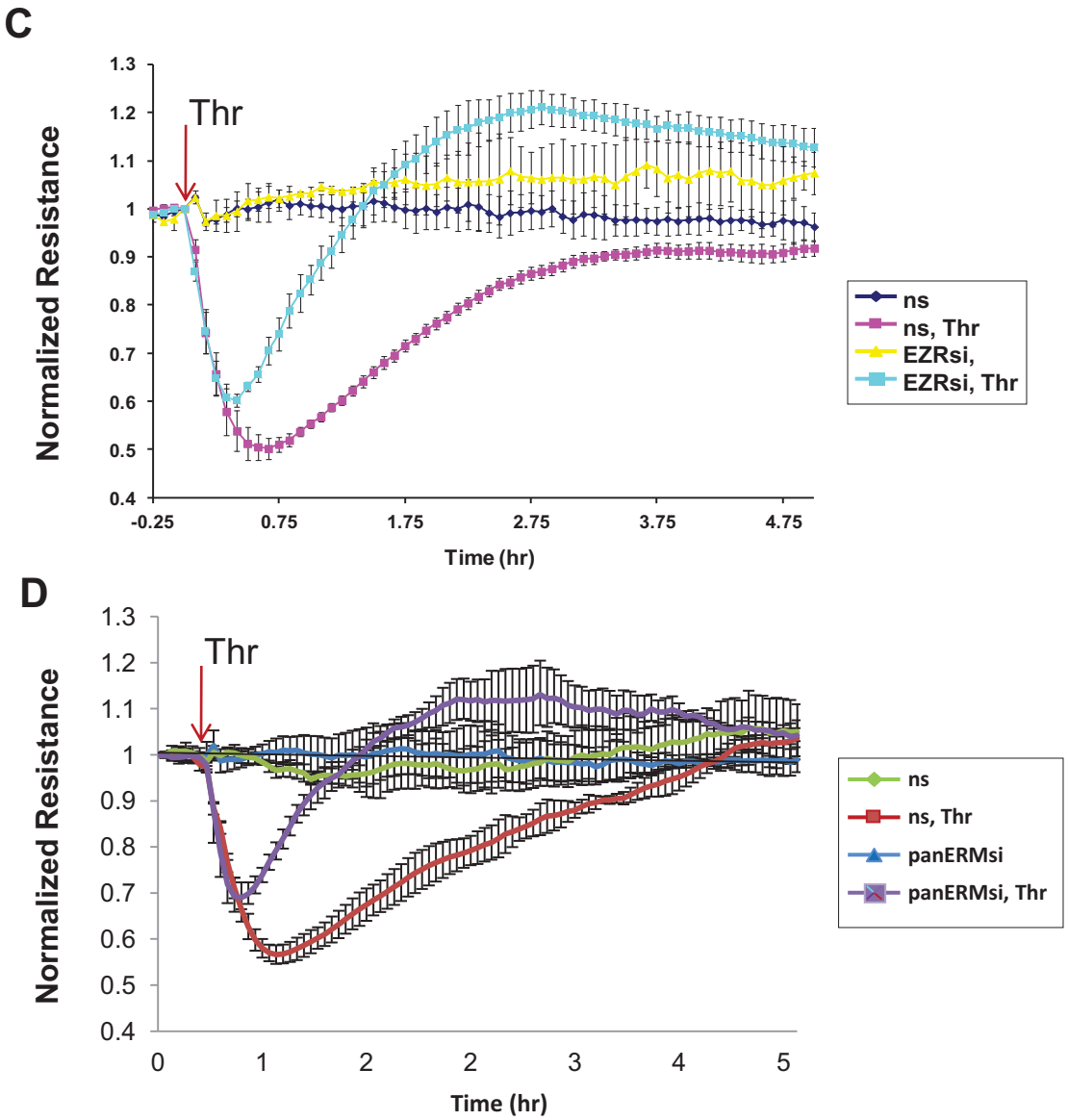
C
Thr
Normalized Resistance
1.3
1.2
1.1
1
0.9
0.8
0.7
0.6
0.5
0.4
-0.25
0.75
1.75
2.75
3.75
4.75
Time (hr)
ns
ns, Thr
EZRsi,
EZRsi, Thr
D
Thr
Normalized Resistance
1.3
1.2
1.1
1
0.9
0.8
0.7
0.6
0.5
0.4
0
1
2
2
3
4
5
Time (hr)
ns
ns, Thr
panERMsi
panERMsi, Thr

Figure 8E

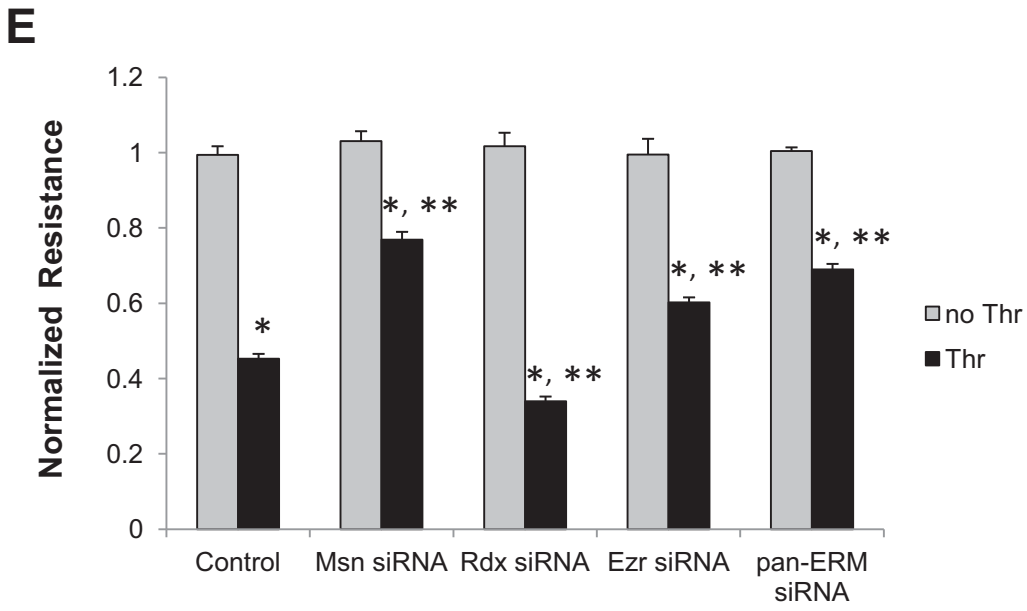
E
Normalized Resistance
1.2
1
0.8
0.6
0.4
0.2
0
*
*, **
*, **
*, **
*, **
Control
Msn siRNA
Rdx siRNA
Ezr siRNA
pan-ERM siRNA
no Thr
Thr

Figure 9

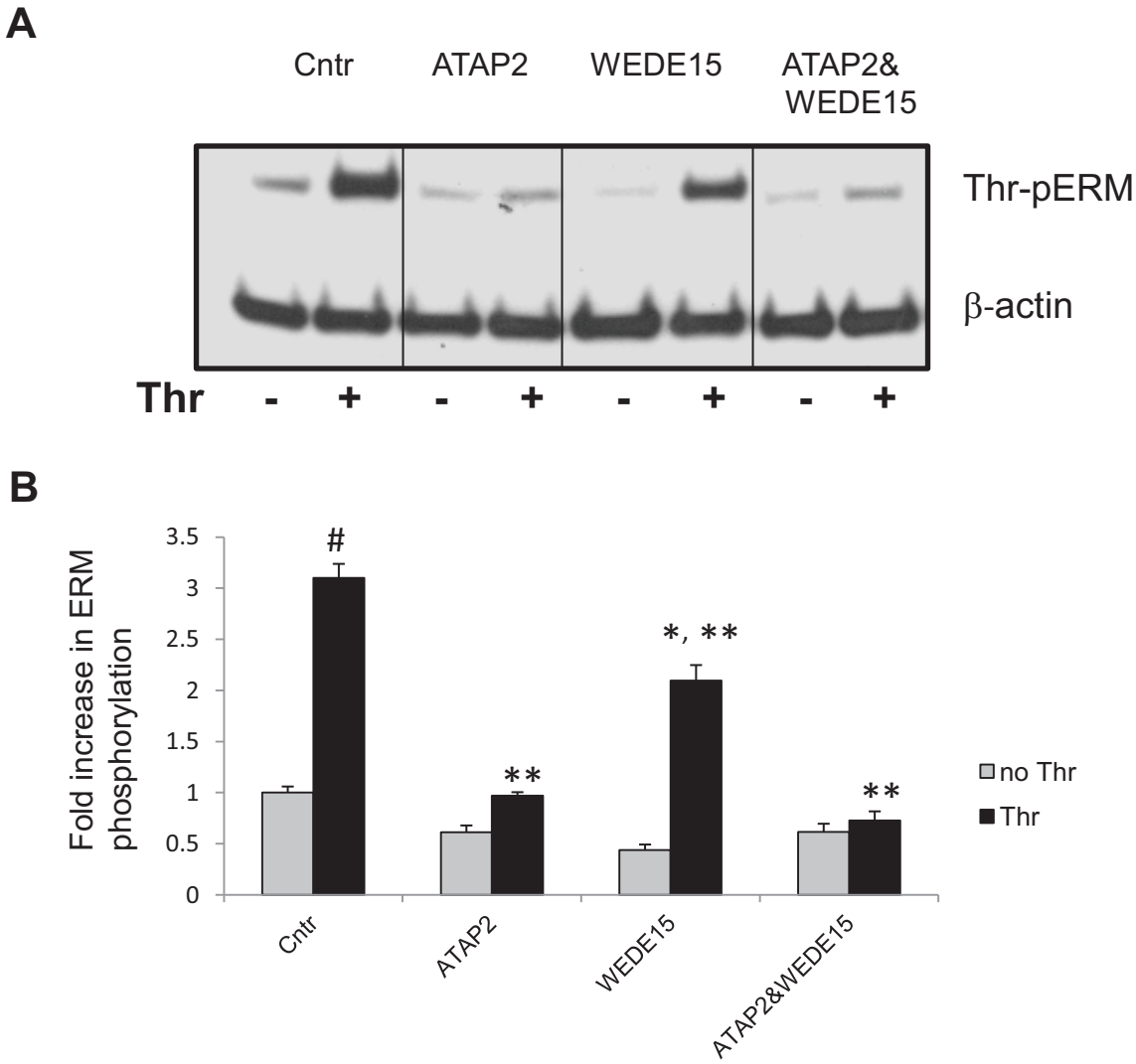
A
Cntr
ATAP2
WEDE15
ATAP2&
WEDE15
Thr-pERM
β-actin
Thr - + - + - + - +
B
Fold increase in ERM phosphorylation
3.5
3
2.5
2
1.5
1
0.5
0
#
*, **
**
**
Cntr
ATAP2
WEDE15
ATAP2&WEDE15
no Thr
Thr

Figure 10

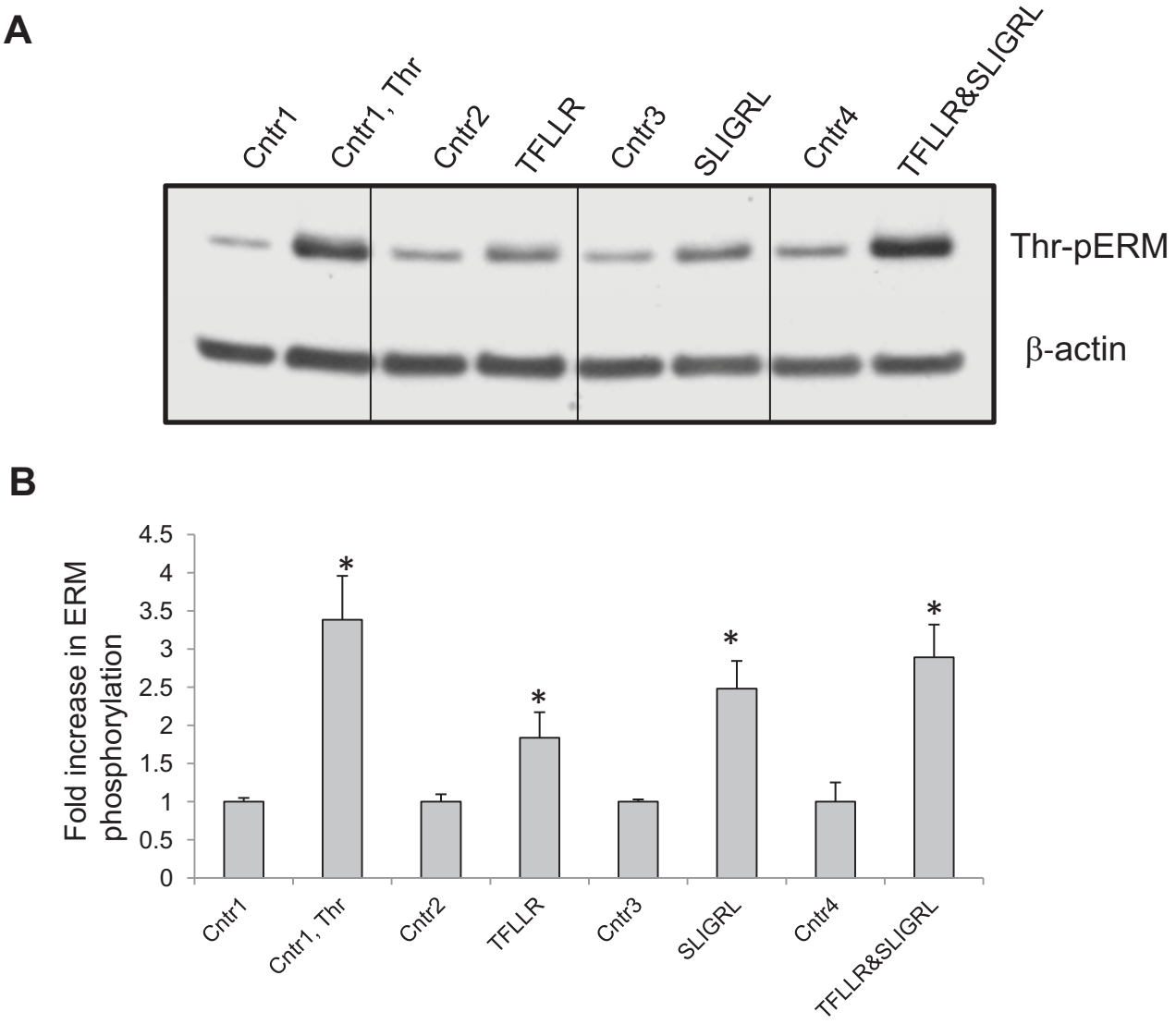
A
Cntr1
Cntr1, Thr
Cntr2
TFLLR
Cntr3
SLIGRL
Cntr4
TFLLR&SLIGRL
Thr-pERM
β-actin
B
Fold increase in ERM phosphorylation
4.5
4
3.5
3
2.5
2
1.5
1
0.5
0
*
Cntr1
Cntr1, Thr
Cntr2
TFLLR
Cntr3
SLIGRL
Cntr4
TFLLR&SLIGRL

Figure 11

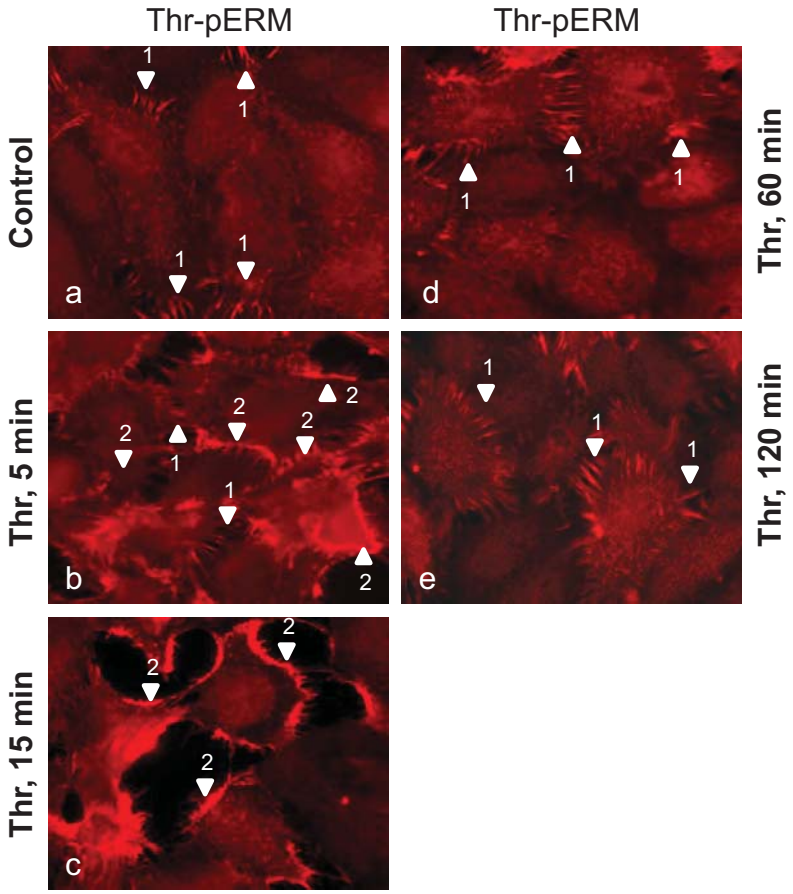
Thr-pERM
Thr-pERM
Control
Thr, 60 min
Thr, 5 min
Thr, 120 min
Thr, 15 min
a
b
c
d
e

Figure 12

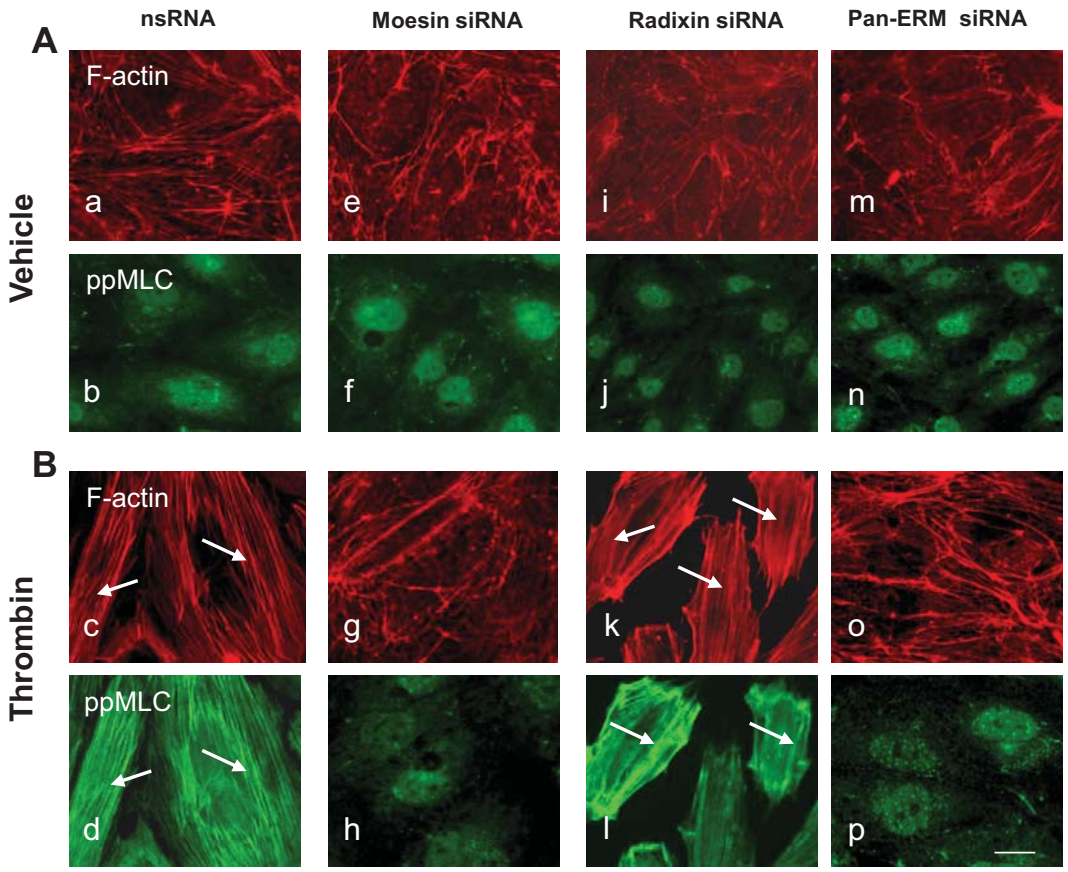
nsRNA
Moesin siRNA
Radixin siRNA
Pan-ERM siRNA
A
Vehicle
F-actin
a
e
i
m
ppMLC
b
f
j
n
B
Thrombin
F-actin
c
g
k
o
ppMLC
d
h
l
p

Figure 13

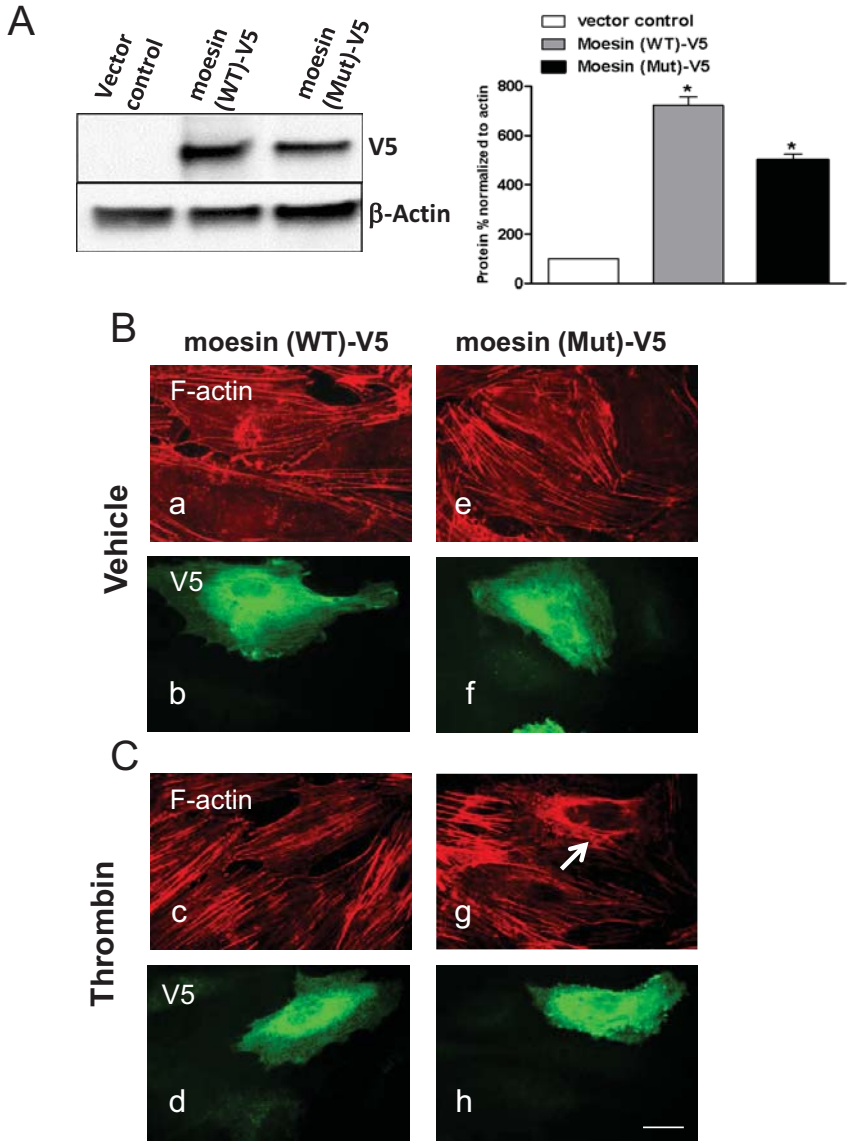
A
Vector control
moesin (WT)-V5
moesin (Mut)-V5
V5
β-Actin
vector control
Moesin (WT)-V5
Moesin (Mut)-V5
Protein % normalized to actin
800
600
400
200
0
*
*
B
moesin (WT)-V5
moesin (Mut)-V5
Vehicle
F-actin
a
e
V5
b
f
C
Thrombin
F-actin
c
g
V5
d
h

Figure 14

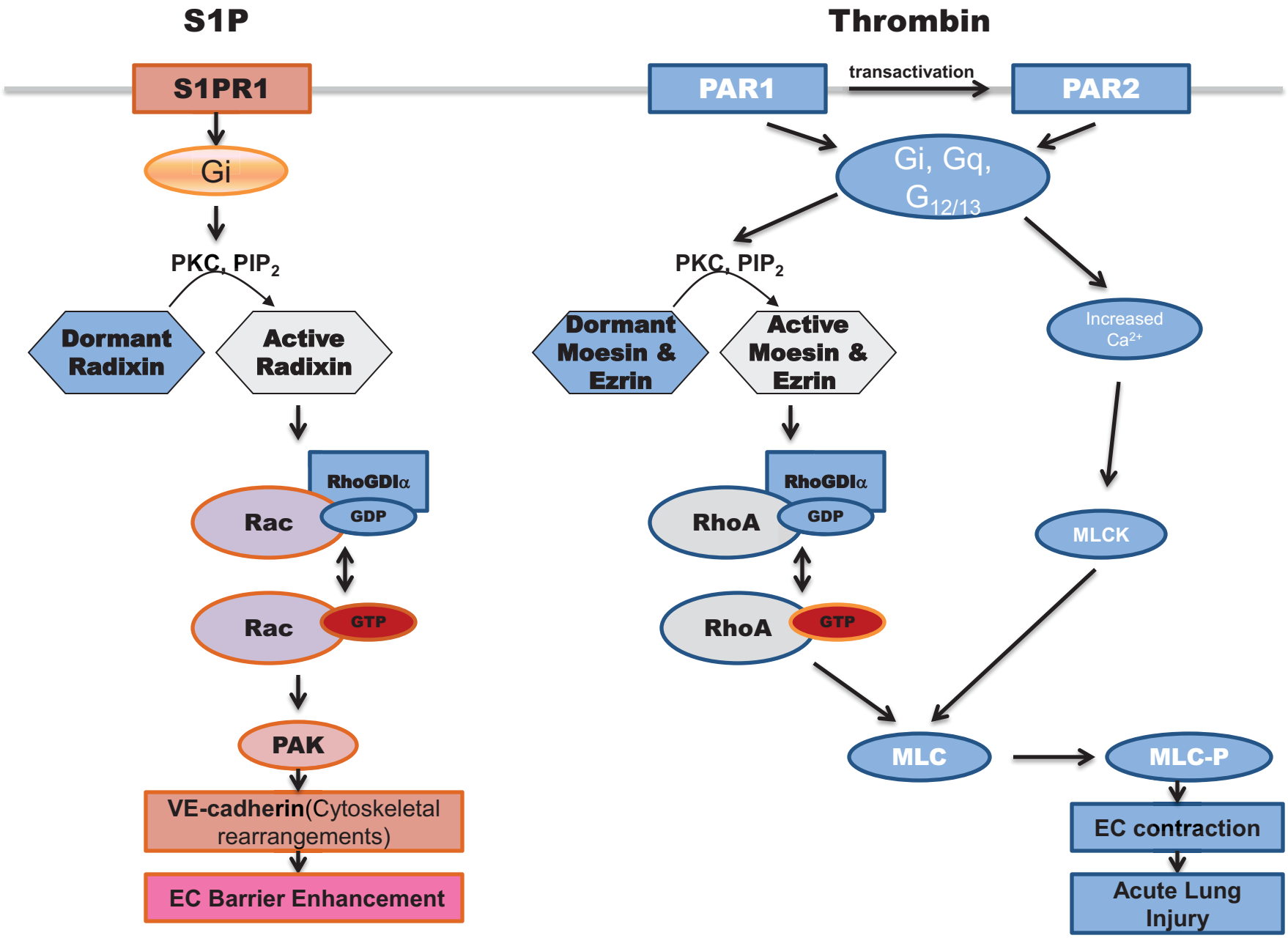
S1P
S1PR1
Gi
PKC, PIP2
Dormant Radixin
Active Radixin
RhoGDIα
Rac
GDP
Rac
GTP
PAK
VE-cadherin(Cytoskeletal rearrangements)
EC Barrier Enhancement
Thrombin
PAR1
transactivation
PAR2
Gi, Gq, G12/13
PKC, PIP2
Dormant Moesin & Ezrin
Active Moesin & Ezrin
Increased Ca2+
RhoGDIα
RhoA
GDP
RhoA
GTP
MLCK
MLC
MLC-P
EC contraction
Acute Lung Injury